HHS Public Access

Author manuscript

Ocul Surf. Author manuscript; available in PMC 2024 October 01.

Published in final edited form as:

Ocul Surf. 2023 October ; 30: 57–72. doi:10.1016/j.jtos.2023.07.008.

Conditional deletion of CD25 in the corneal epithelium reveals sex differences in barrier disruption

Anmar Abu-Romman[1], **Kaitlin K. Scholand**[1,2], **Sonali Pal-Ghosh**[3], **Zhiyuan Yu**[1], **Yashwawini Kelagere**[1], **Ghasem Yazdanpanah**[1], **Winston W-Y Kao**[5], **Vivien J. Coulson-Thomas**[6], **Mary Ann Stepp**[3,4], **Cintia S. de Paiva**[1,2]

[1]Ocular Surface Center, Department of Ophthalmology, Cullen Eye Institute, Baylor College of Medicine, Houston, Texas, United States.

[2]Department of Biosciences, Rice University, Houston, TX, United States.

[3]Department of Anatomy and Cell Biology, The George Washington University School of Medicine and Health Sciences, Washington, District of Columbia, United States.

[4]Department of Ophthalmology, The George Washington University School of Medicine and Health Sciences, Washington, District of Columbia, United States.

[5]Department of Ophthalmology, University of Cincinnati, Cincinnati, OH, United States.

[6]University of Houston, College of Optometry, Houston, Texas, United States.

Abstract

Purpose—IL-2 promotes activation, clonal expansion, and deletion of T cells. IL-2 signals through its heterotrimeric receptor (IL-2R) consisting of the CD25, CD122 and CD132 chains. CD25 knockout (KO) mice develop Sjögren Syndrome-like disease. This study investigates whether corneal CD25/IL-2 signaling is critical for ocular health.

Methods—Eyes from C57BL/6 mice were collected and prepared for immunostaining or in-situ hybridization. Bulk RNA sequencing was performed on the corneal epithelium from wild-type and CD25KO mice. We generated a conditional corneal-specific deletion of CD25 in the corneal epithelium ($CD25^{\Delta/\Delta CEpi}$). Corneal barrier function was evaluated based on the uptake of a fluorescent dye. Mice were subjected to unilateral corneal debridement, followed by epithelial closure over time.

Corresponding author: Cintia S. de Paiva, M.D., Ph.D., Ocular Surface Center, Cullen Eye Institute, Dept. of Ophthalmology, Baylor College of Medicine, 6565 Fannin Street, NC 505G, Houston, TX 77030, cintiadp@bcm.edu.

Author's Contributions: CSdP was involved in the conception of the study; VJC-T and CSdP designed the study; YK, GY, KKS, ZY, SP-G and AA-R were involved in data acquisition; WK donated the Keratin 12 mice ^{rtTA}/tetO-cre mice; CSdP, YK, GP, KKS, ZY, SP-G, and MAS were involved in data analysis and interpretation. CSdP and AA-R drafted the manuscript. VJC-T, MAS, and KKS edited the manuscript. All authors contributed to the article by editing and approving the submitted version.

Declaration of competing interest

CSdP was a consultant for Spring Discovery from May 2022-August 2022, and she has received research contracts from Roche, BioAegis, Serpass and Aerie Pharmaceuticals. None of these are related to the subject of this study. All other authors declare no competing interests.

Results—In C57BL/6 mice, CD25 mRNA was expressed in ocular tissues. Protein expression of CD25, CD122, and CD132 was confirmed in the corneal epithelium. Delayed corneal re-epithelization was seen in female but not male CD25KO mice. There were 771 differentially expressed genes in the corneal epithelium of CD25KO compared to wild-type mice. While barrier function is disrupted in CD25$^{\Delta/\Delta CEpi}$ mice, re-epithelialization rates are not delayed.

Conclusions—All three chains of the IL-2R are expressed in the corneal epithelium. Our results indicate for the first time, deleting CD25 systemically in all tissues in the mouse and deleting CD25 locally in just the corneal epithelium compromises corneal epithelial barrier function, leading to dry eye disease in female mice. Future studies are needed to delineate the pathways used by IL-2 signaling to influence cornea homeostasis.

Keywords

CD25; IL-2; cornea; dry eye; wound healing; sex; corneal barrier

1. Introduction

The cornea is the outer most surface of the eye, and it is responsible for at least 1/3 of the refraction power of the globe. The cornea is highly specialized tissue that is uniquely avascular and must remain transparent. It is richly innervated and responds to various chemical, mechanical, and thermal stimuli to initiate reflex blinking and tearing. Corneal epithelial cells have been found to function as surrogate glial cells for the unmyelinated corneal nerves by phagocytosing damaged nerve endings and stimulating nerve regrowth [1]. Keratin 12 (Krt12), a type I keratin, is specific for the corneal epithelium, and gene mutations in the *Krt12* gene lead to corneal dystrophies and the appearance of microcysts [2]. Using the Cre-Lox system, Keratin12-Cre reverse transcriptase (Krt12^{rtTA}) mice have been bred with tetO-cre mice, and a floxed allele has been used to investigate gene knock-in in the cornea epithelia with high specificity [3-6].

Interleukin-2 (IL-2) is a cytokine with central roles in inflammation and immune signaling on T, B, and natural killer cells, promoting activation, clonal expansion, and deletion of T cells [7]. IL2 signals through the heterotrimeric IL-2 receptor (IL-2R), comprised of an α (CD25), β (CD122), and γ chains (CD132). CD25 is a critical component in IL-2 signaling [7]. CD25 is constitutively expressed in regulatory T cells (Tregs) and transiently upregulated in T cells after activation [8, 9]. Non-immune expression of IL-2R chains has also been reported, such as in some regions of the brain, in minor salivary gland biopsies, fibroblasts, endothelial, and intestinal goblet cells. Certain epithelial cells (intestinal, kidney, and airway) also express CD25 protein [10-19]. We and others have shown that CD25 protein is detected in the cornea [20-22], conjunctiva [20, 22], and CD122 protein is observed in the cornea, conjunctiva, and gut epithelia [20, 23, 24]. It is unknown if the cornea expresses CD132, and the function of local IL-2R expression in these tissues remains elusive.

Tregs constitutively express high levels of CD25 on the surface and are therefore, the most studied cell regarding IL-2 signaling [8, 9, 25-27]. Interestingly, CD25 knock-out (CD25KO) mice develop systemic autoimmunity, colitis, and a severe Sjögren Syndrome-

like disease with ocular and lacrimal gland alterations [20, 28-34]. These changes have been linked to spontaneous activation of T cells that do not undergo activation-induced cell death and loss of Tregs [28, 30, 31, 35]. We recently reported that CD25KO mice display diminished corneal sensitivity and significantly reduced intraepithelial axonal density and stromal nerve arborization compared to wild-type mice [36]. However, the reduction in epithelial axon density occurs prior to the reduction in stromal nerves, indicating the loss in epithelial axon density is likely caused locally and not systemically. Herein we investigate whether a locally expressed IL-2/IL-2R signaling axis is essential for maintaining corneal homeostasis and regulating a corneal wound healing response.

2. Methods

2.1 Animals

The following mouse strains were acquired and used as described below.

1. **CD25KO mice**. Heterozygous CD25 (B6.129S4-*IL-2ra*$^{tm1Dw/}$J strain, stock 2952) mice on the C57BL/6 background aged 6–8 weeks old were purchased from Jackson Laboratories (Bar Harbor, ME). They were housed in our vivarium in a specific pathogen-free environment, and breeding colonies were established. This study used 32 wild-type (20 females, 12 males) and 57 CD25KO mice (32 females and 25 males); all were bred in-house.

2. **Female C57BL/6** mice were purchased from Jackson Laboratories and used at 8 weeks of age (n = 42).

3. **Keratin-12 reporter mouse (*Krt12cre;Ai14)***. *Krt12*^{rtTA} Keratin 12-reverse tetracycline-trans-activator knock-in/tetO-cre (*Krt12*$^{rtTA/rtTA}$/tetO-cre [37, 38] mouse line was obtained from Dr. Winston Kao (Professor at the Dept. of Ophthalmology, University of Cincinnati, Cincinnati, OH) and was bred with tetO-cre from Jackson Laboratories (STOCK Tg(tetO-cre)1Jaw/J, stock number 006224) and Ai14 dtTomato strain (B6.Cg-Gt(ROSA)26Sor$^{tm14(CAG-tdTomato)Hze/}$J, Jackson Laboratories stock 7914), Jackson Laboratories,) to generate *Krt12*$^{rtTA/rtTA}$tetO-cre/Ai14 mice, hereafter referred to as *Krt12cre; Ai14.* For this study, we used four *Krt12cre;Ai14 mice* (two received doxycycline chow and two receive regular chow).

4. **Cornea-specific deletion of CD25.** Using the same cre-Flox system, we generated ternary keratin 12-cornea specific, doxycycline-inducible tetO-cre, CD25 knockout line. For such, we mated the *Krt12*$^{rtTA/rtTA}$tetO-cre described above with the CD25^{flox} mice [B6(129S4)-*Il2ra*$^{tm1c(EUCOMM)Wtsi/}$TrmaJ [9, 39], stock 033093, Jackson Laboratories) to obtain *Krt12*$^{rtTA/rtTA}$/tetO-cre^{+}/CD25$^{flox/flox}$ (ternary mouse), hereafter referred to as *CD25*$^{\Delta/\Delta CEpi}$ and *Krt12*$^{rtTA/rtTA}$/CD25$^{flox/flox}$ (binary mice that do not have cre and were used as littermate controls).

Each transgene allele was identified by PCR genotyping (Transnetyx, Cordova, TN). Cre recombinase expression, under the control of a tetracycline-responsive element, was induced in mice by replacing their regular chow with doxycycline chow (200mg/kg, Bio-Serv,

Flemington, NJ) ad libitum. For such, *Krt12cre;Ai14 mice* were induced at post-natal day 30 or older for two weeks to induce the expression of Ai14. *CD25*$^{\Delta/\Delta CEpi}$ mice were induced at post-natal day 30 or older for eight weeks to induce the irreversible excision of CD25 in Krt12 expressed cells. Double-transgenic (*Krt12*$^{rtTA/rtTA}$/CD25$^{flox/flox}$) cage mates also received a doxycycline diet. For this study, we used 157 mice (53 female *CD25*$^{\Delta/\Delta CEpi}$, *24 male CD25*$^{\Delta/\Delta CEpi}$, 55 female *Krt12*$^{rtTA/rtTA}$/CD25$^{flox/flox}$ and 25 male *Krt12*$^{rtTA/rtTA}$/CD25$^{flox/flox}$).

Institutional Animal Care and Use Committees at Baylor College of Medicine previously approved all animal experiments and procedures. In addition, all studies adhered to the Association for Research in Vision and Ophthalmology for the Use of Animals in Ophthalmic and Vision Research and to the National Institutes of Health guide for the care and use of Laboratory Animals (NIH Publications No. 8023, revised 1978). All experiments were performed at Baylor College of Medicine (Houston, Texas).

2.2 RNAscope

Eyes and adnexa, and spleens from C57BL/6 mice (n = 5) were collected and snap-frozen in OCT and liquid nitrogen. Sections were cut from each frozen block at 5 μm thickness and mounted on positively charged slides (Fisherbrand™ Superfrost™ Plus Microscope Slides, Fisher-Scientific). Slides were prepared for RNA Scope following the manufacturer's protocols for probe hybridization and amplification (RNAscope™ 2.5, RED, Advanced Cell Diagnostics/Bio-techne, Newark, CA) at the Pathology Core at Baylor College of Medicine. The following RNAscope™ probes were used: Mm-*Krt12* (Cat #523671, used as positive control for tissue reaction) and Mm-*Il2ra* (Cat #449341). An Eclipse E400 Nikon fluorescence microscope equipped with a DS–F1 digital camera was used to capture and photograph the bright field images. The captured images were processed using the denoise function in the NIS Elements Advanced Research (AR) software version 4.20 (Nikon, Melville, NY).

2.3 Histology, PAS staining, IHC, and quantification of focus score

Eyes and lacrimal glands were excised, fixed in 10% formalin, paraffin-embedded, and cut into 4-μm sections using a microtome (ThermoFisher, Microm HM 315, Waltham, MA, USA). Sections were stained with hematoxylin and eosin (H&E) or Periodic Acid Schiff (PAS) using an autostainer (Gemeni AS, ThermoFisher, Waltham, MA, USA) and coverslips were applied (Tissue Tek Auto Cover Slipper 4764, Sakura, Torrance, CA) at Precise Pathology Associates, PLLC (The Woodlands, TX). The goblet cell density was measured in the superior and inferior bulbar and tarsal conjunctiva using NIS-Elements software (AR, version 5.20.2; Nikon) and expressed as the number of positive cells per millimeter [40]. Histologic evaluation of H&E-stained lacrimal glands was performed by standard light microscopy using a 10X and 40X objectives (Eclipse E400, Nikon) by two masked observers.

2.4 Human or corneal explant primary cultures

Fresh human corneoscleral tissues (<72 h after death) from donors aged 35–57 years without allergic conditions were obtained from the Lions Eye Bank of Texas (Houston, TX) and cultured per our published protocol.

Murine corneas were excised under a surgical microscope using curved Castroviejo scissors into a supplemented hormonal epidermal medium (SHEM) on wet ice containing 5 μg/ml dispase (Sigma-Aldrich, St. Louis, MO). SHEM media was prepared as a 1:1 media mixture of Dulbecco's Modified Eagle's Medium with high glucose (Sigma-Aldrich) and Ham's F-12 media (Sigma-Aldrich) containing five ng/ml EGF (Thermo Fisher Scientific, Waltham, MA, USA), 0.5 mg/ml hydrocortisone (Sigma-Aldrich), 30 ng/ml cholera toxin A (Sigma-Aldrich), 0.5% DMSO (Sigma-Aldrich), 50 mg/ml gentamicin (Hyclone, GE Healthcare Life Sciences, Marlborough, MA), 1.25 mg/ml amphotericin B (Gibco BRL Products, Grand Island, NY, USA), 1X ITS liquid media supplement (Sigma-Aldrich) and 5% FBS (Hyclone™, Cytiva, Marlborough, MA) using our previous methods [41, 42]. The corneas were cut into four equal pieces, incubated at 37 °C for 15 min, and transferred with sterile forceps into SHEM media without dispase. After approximately 10 min, the pieces were transferred into wells of a 48-well culture plate with their epithelium side up. They were allowed to adhere for several minutes, then covered with 200 μl SHEM media and incubated at 37C in 5% CO2. 200 μl fresh SHEM media was added every three days. At subconfluency (~14 days), cells were lysed with RNA lysis buffer (Qiagen, Valencia, CA), and total RNA was extracted.

2.5 RNA Isolation and digital PCR

Corneal epithelial cells were collected by with a dull blade into RNA lysis buffer (Qiagen) and snap frozen into liquid nitrogen and kept at −80C until ready to be extracted. Spleens were collected (n = 2) placed into complete RPMI media and passed through a nylon mesh. Cells were centrifuged, resuspended into red blood cell lysis, incubated at room temperature for 10 minutes followed by ywashing in complete RPMI media and resuspended into RNA lysis buffer (Qiagen). Total RNA was extracted using a QIAGEN RNeasy Plus Micro RNA isolation kit (Qiagen, Valencia, CA) from corneal epithelium, spleen or murine or human corneal epithelial cultures. The RNA concentration was measured by its absorption at 260/280 ratio using a spectrophotometer (NanoDrop 2000; Thermo Scientific, Wilmington, DE). The cDNA was synthesized using random hexamers and M-MuLV reverse transcriptase (Ready-To-Go You-Prime First-Strand Beads; Amersham Pharmacia Biotech, Inc, Piscataway, NJ), and the DNA concentration was measured with a Qubit spectrophotometer (Life Technologies, Grand Island, NY). Digital polymerase chain reaction (PCR) to detect copy number of mouse *Il2ra* (Mm01340213_m1), mouse *Il2rb* (Mm00434268_m1), mouse *Il2rg* (Mm00442885_m1), human IL2RA (Hs00907777_m1), human IL2RB (Hs01081697_m1) and human IL2RG (Hs00953624_m1) transcripts was performed with a QuantStudio 3D Digital PCR system (Life Technologies) according to the manufacturer's instructions and normalized by the concentration of cDNA. Data are presented as copies/ng of cDNA, as published [43].

2.6 Immunofluorescence staining and confocal microscopy

Eyes and adnexae, lacrimal gland cryosections, or wholemount corneas were fixed in 100% acetone or methanol for 20 minutes at −20C followed by washing with Hank's Balanced Saline Solution (HBSS) for 3x5 min with gentle shaking at room temperature (RT). Tissues were further permeabilized with 0.4% Triton X-100 in HBSS for 30 minutes at RT and gentle shaking. 20% goat serum (Sigma-Aldrich) diluted in HBSS was used for 1 hour of blocking at RT. Then the samples were incubated with primary antibodies (Table 1) diluted in 5% goat serum in HBSS with the mentioned concentrations overnight at 4C with gentle shaking in the dark. The samples were then washed with 0.4% Triton X-100 for 3x6 min at RT with gentle shaking, followed by incubation with secondary antibodies (Table 1) diluted in 5% goat serum/HBSS for 1 hour at RT with gentle shaking in the dark. After that, the samples were washed for 3x10 min with 0.4% Triton X-100 in HBSS and then counterstained with DAPI (1:500 in HBSS) for nuclei staining (30 min at RT in the dark with gentle shaking). Finally, wholemount corneas were washed 3x5 min with HBSS and mounted on flattened slides. Images were visualized using a laser scanning Nikon confocal microscope (Nikon A1 RMP, Nikon) and 0.5 μm Z-step (whole-mount corneas only). The captured images were processed using the denoise function in the NIS Elements Advanced Research (AR) software version 4.20 (Nikon).

2.7 Tight Junction Protein evaluation

All eyes were fixed immediately after enucleation in a paraformaldehyde-containing fixative (1x phosphate-buffered saline solution (PBS), 1% formaldehyde, 2 mmol/L MgCl2, 5 mmol/L ethylene glycol-bis(β-aminoethylether)-N,N,N′,N′-tetraacetic acid (EGTA-), 0.02% NP-40) for 1 hour and 15 minutes at 4°C, followed by two washes for 10 minutes each in 1× PBS containing 0.02% NP40 at room temperature. Tissues were placed in 4:1 methanol: dimethyl sulfoxide for two hours at −20°C and then stored in 100% methanol at −20°C until used for whole-mount staining studies. The back of the eye was cut, and the retina, lens, and iris were removed before staining. Tissues were transferred to a graded Methanol-TritonX-100 series (75%, 50%, and 25% methanol: TritonX-100 for 15, 15, and 10 minutes, respectively). All incubations were performed with gentle shaking and at room temperature unless otherwise specified. The eyes were washed twice in PBS for 30 minutes each, followed by incubation with blocking buffer for two hours. Blocking buffer was made as follows: to 100 mL 1× PBS, 1 g of bovine serum albumin was added, the mixture was stirred for 10 minutes, 1 mL of horse serum was added, and the mixture was stirred for an additional minute. The tissues were incubated overnight with primary antibody diluted in blocking buffer at 4°C. ZO-1 (# sc-33725; Santa Cruz Biotechnology, Dallas, TX, USA). Appropriate secondary DyLite 488 from Jackson Immunobiologicals (West Grove, PA, USA) was immunolabeled. The next day, the tissues were washed five times with PBS and 0.02% Tween 20 (PBST) for one hour each, blocked for two hours, and then incubated with a secondary antibody diluted in blocking buffer overnight at 4°C. The following day, eyes were washed three times with PBST for one hour each, followed by nuclear staining with 4,6-diamidino-2- phenylindole (DAPI) for five minutes, and washed with distilled water. To achieve the best flattening, 4 peripheral incisions were made, the corneas were placed epithelial side-up with mounting media (no. 17984-25, Fluoromount G; Electron Microscopy Sciences, Hatfield, PA, USA) and coverslipped.

All images for analysis were acquired using Nikon Eclipse TS2R at 40x magnification and quantified using NIS Elements BR v5.00. The Nikon elements program was used to draw the area around the cell and ROI area was selected from the settings window in ROI statistics. A minimum of n=300 cells were counted for each genotype. The thickness of the corneal epithelium was assessed for both genotypes at three different sites at the central cornea using the Nikon eclipse Ti2 scope. The ZO1/ DAPI stained flat-mounted corneas were viewed at 40x magnification, and the distance between the apical and basal layers was recorded in microns, as published.[44]

2.8 Western blotting

Cornea, conjunctiva, spleen, and intestine from 8-week-old C57BL/6 mice were harvested and lysed in Buffer A: 0.1M Tris-HCl pH 8.5, 0.15M NaCl, 0.5mM MgCl2, 0.5% NP-40, plus 20mg/ml Pefabloc SC plus (Sigma-Aldrich) and HALT phosphatase inhibitor cocktail (1:100) (ThermoFisher) or Buffer B: 0.1M Tris-HCl pH 8.5, 0.15M NaCl, 0.5mM MgCl2, 0.5% NP-40, plus 2.5mM GM6001 (Sigma-Aldrich). Protein concentration was measured using a micro-BCA protein assay kit (ThermoFisher). Proteins (40μg) were resuspended in SDS sample buffer, boiled for 5 min, and analyzed on 4–15% mini-protean TGX stain-free gels (Bio-Rad, Hercules, CA). The proteins were electrophoretically transferred to polyvinylidene difluoride membranes (Bio-Rad). The blots were probed with a rat anti-mouse CD25 antibody (clone 7D4, BioLegend, San Diego, CA) or an anti-actin antibody (Sigma-Aldrich) overnight at 4C. The blots were washed extensively with a solution containing 50 mM Tris, pH 8.0, 138 mM NaCl, 2.7 mM KCl, and 0.05% Tween 20. The Amersham ECL™ chemiluminescence reagent (GE Healthcare, Chicago, IL) was used to detect antigen/antibody complexes following horseradish peroxidase-conjugated goat anti-mouse IgG as a secondary antibody. Images were taken by ChemiDoc Touch Imaging Systems (ChemiDoc Touch Imaging Systems, Bio-Rad) and processed using Bio-Rad software (Image lab 6.0, Bio-Rad).

2.9 Spleen weight and flow cytometry analysis

Spleens were surgically removed after euthanasia and weighed using a scientific scale (OA84, Ohaus Corporation, Woburn, MA). A single-cell suspension was prepared, as previously shown [45, 46], blocked with CD16/CD32 (BioLegend), washed, and stained with an infra-red fluorescent reactive dye (Life Technologies, Grand Island, NY) before incubation with a Foxp3 Fixation/Permeabilization working solution (eBioscience, ThermoFisher) for 1h. The following antibodies were used: CD4_FITC (clone GK1.5, BD Biosciences, Franklin Lakes, NJ), CD25_PE (clone 7D4, BioLegend), CD45_Alexa Fluor®700 (clone 30F11, BioLegend). The gating strategy used was as follows: two subsequent singlet gates excluded doublets, followed by dead cell exclusion by using live fixable infrared dye. $CD45^+$ cells and subsequently $CD4^+$ T cells were gated, and the frequency of $CD4^+CD25^+$cells was calculated as a percentage of total $CD4^+$ T cells. Negative controls consisted of fluorescence minus one splenocytes. Cells were acquired with a BD Canto II Benchtop cytometer with BD Diva software version 6.7 (BD Biosciences). At least 100,000 events or more were collected. Final data were analyzed using FlowJo software version 10 (Tree Star Inc., Ashland, OR).

2.10 Measurement of corneal barrier function

Corneal barrier function was assessed by quantifying corneal epithelial permeability to 70-kDa Oregon-Green-Dextran-AlexaFluor-488 (OGD; Invitrogen/Thermofisher), according to a previously published protocol [47, 48]. Briefly, 1μL of a 50mg/mL solution of OGD was instilled onto the ocular surface 1 minute before euthanasia with excess isofluorane followed by cervical dislocation. Corneas were rinsed with 2 mL of PBS and photographed with a stereoscopic zoom microscope (model SMZ 1500; Nikon) under fluorescence excitation at 470nm. OGD staining intensity was graded in digital images by measuring the mean fluorescence intensity within a 2-mm diameter circle placed on the central cornea using NIS Elements software (version AR, 5.20.02) by two masked observers. The mean intensity of the right and left eyes was averaged, and the mean average from biological replicates was calculated and analyzed.

2.11 Bulk RNA sequencing and data analysis

Corneal epithelia were collected by scraping female wild-type and CD25KO mice corneas (both 8-week-old, n = 5/group) and from 12-week-old CD25$^{\Delta/\Delta Cepi}$ that received doxycycline chow for 8 weeks (n = 5). Total RNA was extracted using a QIAGEN RNeasy Plus Micro RNA isolation kit (Qiagen) according to the manufacturer's instructions. The concentration and purity of RNA were assessed using a NanoDrop 1000 (ThermoFisher).

A double-stranded DNA library was created using 100ng of total RNA (measured by pico green). First, an oligodT primer containing an Illumina-compatible sequence at its 5' end is hybridized to the RNA, and reverse transcription is performed using a Lexogen kit. Next, second-strand synthesis is initiated by a random primer containing an Illumina-compatible linker sequence at its 5' end. The purified double-stranded library was then amplified and purified. The resulting libraries were quantitated using Qubit 2.0 and fragment size was assessed with the Agilent Bioanalyzer. A qPCR quantitation was performed on the libraries to determine the concentration of adapter-ligated fragments using Applied Biosystems ViiA7 Real-Time PCR System and a KAPA Library Quant Kit (Waltham, MA). All samples were pooled equimolarly, requantitated by qPCR, and re-assessed on the Bioanalyzer. Using the concentration from the ViiA7 ™ qPCR machine above, 1.8pM of the equimolarly pooled library was loaded onto NextSeq 500 high-output flow cell. PhiX Control v3 adapter-ligated library (Illumina, San Diego, CA) was spiked in at 1% by weight to ensure balanced diversity and to monitor clustering and sequencing performance. A single-read 75 bp cycle run was used to sequence the flow cell. An average of 21 million reads per sample was sequenced. The FastQ file generation was executed using Illumina's cloud-based informatics platform, BaseSpace Sequencing Hub.

Data were analyzed by ROSALIND® (https://rosalind.bio/), with a HyperScale architecture developed by ROSALIND, Inc. (San Diego, CA). Reads were trimmed using cutadapt [49] and quality scores were assessed using FastQC. Reads were aligned to the Mus musculus genome build GRCm38 using STAR.[50] Individual sample reads were quantified using HTseq [51] and normalized via Relative Log Expression (RLE) using the DESeq2 R library. [52] Read distribution percentages, violin plots, identity heatmaps, and sample MDS plots were generated as part of the QC step using RSeQC. [53] DEseq2 was also used to calculate

fold changes and p-values and perform optional covariate correction. The clustering of genes for the final heatmap of differentially expressed genes was done using the partitioning around medoids method using the fpc R library. Hypergeometric distribution was used to analyze the enrichment of pathways, gene ontology, domain structure, and other ontologies. The topGO R library[54], was used to determine local similarities and dependencies between GO terms to perform Elim pruning correction. Several database sources were referenced for enrichment analysis, including Interpro [55], NCBI [56], MSigDB [57] REACTOME [58], and WikiPathways [59]. Enrichment was calculated relative to a set of background genes relevant to the experiment.

2.12 Biological pathway analysis using Gene Ontology, Metascape, and Ingenuity Pathways

From the list of differentially expressed genes (DEGs) identified by RNAseq, we used the Gene Ontology database (http://geneontology.org/) to identify the altered biological and cellular pathways. Data was submitted to Metascape (https://metascape.org), a web-portal provides a comprehensive gene list annotation and analysis resource for experimental biologists [60]. To achieve this, we submitted the lists of DEGs and performed a GO enrichment analysis. Then, we selected only the top 10 biological pathways based on fold enrichment with a false discovery rate (FDR) < 0.05. A list with DEGs was also submitted to Qiagen's Ingenuity Pathway Analysis (IPA) system for core analysis. Analysis was performed with an experimental FDR of < 0.05. Only pathways with a Z score ≥ 1 or < than −0.33 (5 pathways) with a −log10 value of >1 and <-1 were chosen. Finally, heatmaps of significantly altered pathways were generated using GraphPad Prism (version 9.2, GraphPad Software, San Diego, CA). Venn diagrams were made using Venny 2.1 [61] https://bioinfogp.cnb.csic.es/tools/venny/)

2.13 Tear washings and multiplex cytokine immunobead assay

Tear washings were collected from female C57BL/6, CD25KO, $CD25^{\Delta/\Delta Cepi}$ and $Krt12^{rtTA/rtTA}/CD25^{f/f}$ mice. $CD25^{\Delta/\Delta Cepi}$ and $Krt12^{rtTA/rtTA}/CD25^{f/f}$ mice received doxycycline diet for eight weeks and were used at 12 weeks of age. Briefly, 1.5 μL of phosphate-buffered saline (PBS, Corning Inc, Manassas, VA) containing 0.1% bovine serum albumin was instilled into the conjunctival sac. The tear fluid and buffer were collected with a 1μL volume glass capillary tube (Drummond Scientific Co, Broomhall, PA) by capillary action from the tear meniscus in the lateral canthus and stored at −80°C until the assay was performed, as published [62]. One sample consisted of pooled tear washings from both eyes of two mice (4 μL) in PBS with 0.1% bovine serum albumin (6 μL). Samples were added to wells containing the appropriate cytokine bead mixture that included mouse monoclonal antibodies specific for VEGF (Millipore, Burlington, MA), as previously reported [46]. The reactions were detected with streptavidin-phycoerythrin using a Luminex 100 IS 2.3 system (Austin, TX). Results were presented as mean±SD (pg/mL). The minimum level of detection was 1.5 pg/ml (VEGF).

2.14 Corneal wound epithelial debridement

Young adult (8-week-old) wild-type mice (15 females, 12 males) and littermate CD25KO mice (12 females, 9 males) were subjected to unilateral epithelial debridement under general

anesthesia using an isoflurane vaporizer (SomnoSuite machine, Kent Scientific Corporation, Torrington, CT). Briefly, after anesthesia, a drop of topical proparacaine was applied to the eye and blotted dry with a filter paper. Next, the central corneal epithelium was demarcated with a 1.5-mm trephine (McKesson Medical-Surgical Inc, Richmond, VA) followed by removal of the epithelium using a sterile disposable blunt blade under a dissecting microscope. Mice were given a special diet of carprofen (2mg/tablet, 1 tablet/mouse/day, Bio-Serv, Flemington, NJ) 24 hours before the procedure to 48 hours after the debridement. No eye drops (whether antibiotics or other treatments) were used.

2.15 Rate of epithelial wound closure

To assess wound size post-injury, 1 μL of 0.1% sterile sodium fluorescein solution in PBS was applied to the wounded eye followed by rinsing of the ocular surface with 1 mL in the temporal side and 1 mL in nasal side of Balanced salt solution (BSS, Alcon Laboratories Inc, Fort Worth, TX) and drying with a filter paper. The cornea was photographed under the LZM microscope (Nikon SMZ1500, Nikon) under an excitation of 488nm with a LED light source (Lumencor Inc, Beaverton, OR) at different time points (1, 20-, 24-, 28, and 48-hours post-injury) using a digital camera (Zyla sCMOS, Andor Technologies, United Kingdom). Image analysis was performed using NIS-Elements imaging software (Advanced research version 5.30.04, Nikon Instruments Inc). Wound size measurements were transferred to an Excel database, where the results were averaged within each group and analyzed. The healing rate was calculated by measuring the re-epithelization area compared to the 1-hour time point area after the epithelial debridement, which was set to 100%.

2.16 Evaluation of corneal barrier function and residual haze 14 days post-injury.

Mice were euthanized on day 14 post-wound, followed by image studies on right and left eyes. First, 2μl of 0.1% sodium fluorescein stain was applied, followed by rinsing the ocular surface with BSS. Fluorescein staining gray levels of the right and left corneas were visualized and photographed under the LZM microscope with a LED light source at an excitation level of 488nm. Then, color imaging was done to both eyes under the LZM microscope with a color digital camera (Zyla sCMOS, Andor Technologies) and high-intensity illuminator (NI-150, Nikon Instruments Inc) to examine for the presence of corneal opacity. Eyes that had corneal opacity were counted and cumulative data was submitted for statistical analysis using the Chi-Square test. These eyes were also excluded from the evaluation of corneal barrier function at day 14.

2.17 Statistical analysis

Statistical analyses were performed with GraphPad Prism software (version 9.4.1, GraphPad Software, San Diego, CA). Data were first evaluated for normality with the Kolmogorov-Smirnov normality test. Then, appropriate parametric (T-test) or non-parametric (Mann-Whitney) statistical tests were used to compare groups. Whenever adequate, one-way or two-way ANOVA or Kruskal-Wallis followed by post hoc tests were used. Frequency of corneal opacification in the groups was evaluated using the Chi-Square test. The final sample per experiment is shown in the Figure legends.

3. Results

3.1 CD25 mRNA is expressed in many ocular tissues

We and others have previously shown that CD25 protein is detected in the corneal epithelium [20, 21]. However, the presence of mRNA in the cornea and other ocular tissues has not been investigated. Herein, we performed in-situ hybridization with eye and adnexae sections using RNAscope (Fig. 1A). We observed mRNA expression in the cornea epithelium and conjunctiva (with greater expression in the cornea than in the conjunctiva) and weak expression in the Meibomian glands.

Next, we collected the corneal epithelium (by scraping) and lysed it into RNA lysis buffer. Spleens were also collected, dissociated into single-cell suspensions, and prepared for gene expression analysis. Absolute quantification of IL-2R chains was performed using Digital PCR as described in the methods and per our previous publication [63]. Absolute quantification by digital PCR is made possible by thousands of individual reactions running in parallel using a chip etched with 20,000 consistently sized nanoscale reaction wells. Samples were normalized to the cDNA amount. Spleens were used as positive controls since they have a high frequency of Tregs ($CD4^+CD25^+$ cell) and other immune cells expressing IL-2Rβ and IL-2Rγ. Results in Fig. 1B demonstrate that all three IL-2R chains are expressed in the murine corneal epithelia and spleen.

To rule out that the expression of IL-2R chains in Fig 1B might have been contaminated with immune cells potentially collected with the corneal epithelial cells, we cultured primary murine and human cornea cells using explants. Cells were grown for 14 days in culture, without exposure to air or any other differentiation media [64-66], after which cells were lysed, total RNA isolated, and subjected to digital PCR as shown in Fig. 1B. Both murine and human primary corneal epithelial cells express all three IL-2R chains (Fig. 1C), confirming epithelial expression of IL-2R chains. These results agree with our previous publication showing CD25 protein expression in freshly collected human cadaveric corneas and in human primary corneal cultures [20].

3.2 All three chains of IL-2 receptors are expressed in the cornea

We confirmed the protein expression of CD25 using cryosections and whole-mount corneas. CD25 protein is clearly expressed in the corneal epithelium (see co-staining with Krt12 in Fig. 2A). Laser confocal microscopy in whole-mount corneas showed that the CD25 expression is at the cellular membrane and has some cytoplasmic staining in the most apical cell layers and is mostly expressed at the wing cell layer, while it is absent in the basal cell layer. (Fig. 2B). No intraepithelial nerve co-localization was observed.

Like the mRNA expression, we observed CD25 protein expression in the Meibomian gland and the lacrimal gland acinar cells (Fig. 2C). Active IL-2 secretion has been proposed to exist in tears, since there is IL-2 immunoreactivity in acinar and ductal epithelial cells of the lacrimal gland [22, 67] and IL-2 is detectable in the tears of healthy subjects [68-73].

We then performed western blots on corneal epithelia, conjunctiva biopsies, spleens, and small intestine. A 55kDa band was observed in the cornea and spleen, while it was

weaker in the conjunctiva and intestine (Fig. 2D). Interestingly, we also observed ~25kDa and ~165kDa bands. These extra bands suggest proteolytic cleavage of the protein and heterodimers, respectively (Fig. 2D). To prevent proteolytic cleavage, we repeated the western blot using another lysis buffer (buffer B described in the methods) and we found similar results (Supplemental Fig. 1). Fowell and colleagues showed that the antibody anti-CD25 clone 7D4 recognizes the p55 and smaller fragments such as 37kDa, 22kDa, and 18kDa [74]; therefore we believe that the antibody correctly identifies all bands in our Fig. 2D.

Using immunofluorescence, we verified the protein expression of the other IL-2R chains. There was immunoreactivity in the corneal epithelium for IL-2Rβ (CD122) and IL-2Rγ (CD132) (Fig. 2E), in agreement with the mRNA expression observed with the digital PCR in Fig. 1D. Taken together, these results validate the expression of all IL-2R chains at the mRNA and protein level in the corneal epithelium.

3.3 Altered transcriptome changes in CD25KO corneal epithelium

To increase our knowledge of the altered pathways in the corneal epithelium of CD25KO mice compared to C57BL/6 mice, we collected corneal epithelium by scraping corneas from female CD25KO and wild-type littermate mice aged eight weeks (n = 5/group). Total RNA was extracted and subjected to bulk RNA sequencing. Data were analyzed using ROSALIND (Fig. 3A). In this analysis, 771 DEGs with a fold change of at least 1.5 and a false discovery rate (FDR) < 0.05 were identified; of these, 551 DEGs were upregulated while 260 were downregulated (Fig. 3B, Supplemental File 1). A volcano plot graphically shows the gene distribution between the two groups. The DEGs that passed FDR were further analyzed using Ingenuity Pathway Analysis. There were 27 differentially modulated pathways with a Z score ≥ 1 (22 pathways) or < than −0.33 (5 pathways) with a −log10 value of >1 and <−1. The Z score infers the likely activation or downregulation state of a given pathway based on the upregulation or downregulation of genes in our sets in comparison to expected changes the IPA database. Necroptosis, a cell death pathway recently described in corneal epithelial cells [75], had the highest Z score (2.8, Fig. 3C). The next consecutive pathways with positive Z scores (indicating upregulation) were glycolysis I, oxidative phosphorylation, immunogenic cell death signaling, and insulin secretion signaling. Among the remaining 22 pathways with positive Z score (Supplemental File 2), we included neutrophil extracellular trap signaling (Z score 2=2.3) and autophagy (Z-score = 1. 14). These two pathways have been reported in dry eye [36, 76]. Pathways with negative Z-scores include synaptic long-term depression (Z score = −0.6), ATM signaling (Z-score = −1.3) and mitochondrial dysfunction (Z-score = −1.6)” (Fig 3C). Additional pathways are shown in Supplemental File 2. Long-term depression happens when synapses become less efficient in transmitting neuronal signals [77]. ATM (Ataxia Telangiectasia Mutated) is a kinase that coordinates the cellular response to DNA damage. The genes involved in these pathways in our dataset can be seen in Fig. 3D and 3E. Interestingly, despite having a Z-score indicative of downregulation, most of the genes in the long-term synaptic depression and mitochondrial dysfunction pathways were upregulated, indicating that the upregulation of these DEGs participates in the predicted downregulation of the pathway.

We also performed a graphical summary of our DEGs (Supplemental Fig. 2). It was predicted that IL-1β, TNF, IFN-γ, IL-6, and IL-5 were upregulated, indicating increased immune and inflammatory mediators in the cornea. This prediction agrees with the immunological pathways that were identified (Fig. 3D, 3E). Nodes with upregulated transcription regulators include ATF4, STAT3, SREBF1, SREBF2, MYC, and SRE. Predicted inhibition involved POR (cytochrome p45o oxidoreductase), an enzyme involved in the terminal complex of eukaryotic oxidative phosphorylation in mitochondria. The complete list of altered pathways can be found in Supplemental File 2.

We also subjected all DEG lists to gene ontology analysis. The biological and cellular processes that are either upregulated or downregulated are shown in Supplemental Fig. 3 and Supplemental File 3. These findings indicate that lack of CD25/IL-2 alters corneal epithelium biology.

3.4 CD25KO mice have delayed corneal re-epithelization after corneal epithelial wound debridement

To determine whether the deficiency of CD25 impacts corneal epithelial wound healing in mice, we assessed corneal re-epithelization in CD25KO (9 females and 12 males) and wild-type mice (15 females and 12 males). A 1.5 mm wound was created in the center of the cornea under general anesthesia with isoflurane (as described in the methods). Wound closure was followed using image analysis in corneas stained with 0.1% fluorescein at 1h, 6h, 20h, 24h, 28h, and 48 h post-injury (Fig. 4A). The corneal re-epithelialization rate in CD25KO female mice was significantly delayed at 20, 24, 28, and 48h compared to the wild-type (both male and female) and CD25KO male mice (Fig. 4B). These results indicate a defect in corneal re-epithelization in CD25KO female mice after injury.

After the initial 48h, mice were returned to their cages. In addition to autoimmune dry eye, CD25KO mice have reduced lifespan [28]. Due to these comorbidities, our final assessment of these mice was performed at 2 weeks after wounding. We evaluated the corneal barrier function and presence of persistent epithelial defects two weeks after the initial injury in all CD25KO mice that reached 10 weeks of age (7 females, 5 males, Fig. 4C). Because we did not acquire the non-wounded eye images in our initial studies, only 11 WT female mice were included on the day 14 evaluation. 3/7 of CD25KO female mice (Fig. 4C) and 1/11 WT female mice (not shown) had open wounds at day 14. There were no open wounds in the male group. Consistent with the delayed re-epithelization seen at 48h post-injury, female CD25KO mice (n = 7) had the worst corneal barrier function at day 14 compared to wild-type female (n = 11), wild-type male (n = 12) and CD25KO male (n = 5); this was only present in the eye that was wounded (Fig. 4C, 4D). Bright-field imaging of wounded eyes showed that corneal opacification was present in 2/7 CD25KO female mice (one mouse had a grade 1 and another had a grade 2). In contrast, no signs of corneal haze/corneal opacification were present in the other groups (Fig. 4E). These findings indicate that either a lack of CD25/IL-2 epithelial signaling or immune activation due to systemic activation impacts the cornea response to epithelial injury and repair.

3.5 Conditional deletion of CD25 in the corneal epithelium leads to spontaneous ocular surface disease

Since CD25 is highly expressed in Tregs, and lack of Tregs leads to autoimmunity, it has been impossible to differentiate between the impact of systemic autoimmunity and the lack of corneal epithelial IL-2 signaling *in vivo.* Therefore, to dissect individual contributions from an overly active immune system or the local loss of IL-2 corneal signaling *in vivo,* we created a corneal epithelial cell-specific CD25 deletion using the Cre-Lox system, as described in the methods. We also created a Krt12 reporter mouse by mating the $Krt12^{rtTA/rtTA}/TC^{+}$ with Ai14 dtTomato, evidencing the cells in the corneal epithelium that would lack CD25 (Supplemental Fig. 4A), as previously shown [37]. With this model, mice lack CD25 expression exclusively in the corneal epithelium without presenting systemic autoimmunity, herein referred as $CD25^{\Delta/\Delta CEpi}$. Mice were fed doxycycline chow at 4 weeks of age for 8 weeks and evaluated at 12 weeks, which led to the successful ablation of CD25 in the corneal epithelium (Supplemental Fig. 4B). $CD25^{\Delta/\Delta CEpi}$ mice were compared to non-induced ternary mice (mice without a doxycycline diet) and to binary mice that were fed doxy chow.

To confirm $CD25^{\Delta/\Delta CEpi}$ mice do not present autoimmunity, as observed with the CD25KO mice, we analyzed the frequency of $CD4^{+}CD25^{+}$ cells (Tregs) in the spleens of the mice. As expected, the frequency of Tregs in the $CD25^{\Delta/\Delta CEpi}$ and binary control mice were not different from each other, while splenocytes from the CD25KO mice had minimal Treg numbers (Supplemental Fig. 4C). Since the enlargement of lymphoid organs is a characteristic of CD25KO mice [28], we collected and weighed spleens from $CD25^{\Delta/\Delta CEpi}$, and $Krt12^{rtTA/rtTA}/CD25^{f/f}$ mice. There was no difference between the $CD25^{\Delta/\Delta CEpi}$ *and* $Krt12^{rtTA/rtTA}/CD25^{f/f}$ spleen mass, but both groups were significantly different from the CD25KO mice, which have enlarged spleens due to clonal expansion of autoreactive T cells (Supplemental Fig. 4D). These findings confirm that there is no effect on the immune cells (Tregs), characteristic of the CD25KO mice, in $CD25^{\Delta/\Delta CEpi}$ mice.

To rule out any immune infiltration in the lacrimal glands, another hallmark phenotype of CD25KO mice, lacrimal glands were collected from $CD25^{\Delta/\Delta CEpi}$ and $Krt12^{rtTA/rtTA}/CD25^{f/f}$ mice and histologic sections were prepared. No lacrimal gland infiltration or acinar alterations were observed in H&E-stained lacrimal glands (not shown). Meibomian gland morphology also appeared normal (not shown). Because we reported that VEGF-A is decreased in the tears of aged mice [46, 62], we assayed tear VEGF-A levels as a proxy for lacrimal gland function. We included naïve C57BL/6J and CD25KO mice as additional controls. CD25KO mice have severe lacrimal gland infiltration and fibrosis [33, 34], so we hypothesized that those mice would have very low levels of VEGF-A in tears. Consistent with the normal lacrimal gland architecture, $CD25^{\Delta/\Delta CEpi}$ mice had VEGF-A levels like binary controls and C57BL/6 mice, while levels were decreased in the CD25KO mice (Fig. 5A). These results validate $CD25^{\Delta/\Delta CEpi}$ as a tissue-specific CD25 deletion in the cornea without systemic effects.

Next, we evaluated the cornea barrier function of $CD25^{\Delta/\Delta CEpi}$ and $Krt12^{rtTA/rtTA}/CD25^{f/f}$ mice at 12 weeks of age (after eight weeks of doxycycline diet) using the uptake of Oregon-Green-Dextran dye (70,000 MW) in both male and female mice. Only female $CD25^{\Delta/\Delta CEpi}$

mice showed increased corneal barrier disruption (Fig. 5B) compared to male CD25$^{\Delta/\Delta CEpi}$ mice and cage mates Krt12$^{rtTA/rtTA}$/CD25$^{f/f}$ mice.

We have reported that mice subjected to desiccating stress have altered corneal barrier function and a parallel disturbance in tight junction protein distribution (such as Zonula occludens-1 [ZO-1] and occludin) and net-like formation [78]. Therefore, we stained wholemount corneas from CD25$^{\Delta/\Delta CEpi}$ and Krt12$^{rtTA/rtTA}$/CD25$^{f/f}$ using a ZO-1 antibody. We measured apical squame area as previously shown [79]. Representative images are shown in Fig. 6. We observed that CD25$^{\Delta/\Delta CEpi}$ had larger apical squame area (Fig. 6A, B) but similar epithelial thickness and ZO-1 thickness compared to Krt12$^{rtTA/rtTA}$/CD25$^{f/f}$ corneas. So, despite the altered function of the corneal barrier, no obvious morphological changes were seen with ZO-1 immunolocalization.

Taken together, these results show CD25$^{\Delta/\Delta CEpi}$ mice do not have enlarged spleens and have a normal frequency of Tregs. However, female CD25$^{\Delta/\Delta CEpi}$ mice display a spontaneous dry eye corneal phenotype, despite normal lacrimal gland and Meibomian gland architecture and normal lacrimal gland function. Furthermore, these findings indicate that disruption of CD25/IL-2 signaling at the corneal epithelium is sufficient to induce a dry eye phenotype in female mice.

3.7 Cornea-specific deletion of CD25 does not affect wound healing after corneal debridement but leads to residual barrier disruption post-wound

Next, we performed corneal epithelial debridement experiments in female CD25$^{\Delta/\Delta CEpi}$ and Krt12$^{rtTA/rtTA}$/CD25$^{f/f}$ mice (Fig. 7A). As before, mice were subjected to a unilateral epithelial debridement and followed for the first 48h of wound closure using fluorescein staining. The rate of re-epithelization was similar in both groups (Fig. 7B). Evaluation of the barrier function at day 14 post-injury showed that CD25$^{\Delta/\Delta CEpi}$ mice had worse barrier function than control mice. There was no difference in the frequency of corneal opacifications among the two groups (4/18 in the CD25$^{\Delta/\Delta CEpi}$ and 6/16 on the Krt12$^{rtTA/rtTA}$/CD25$^{f/f}$ group, non-significant Chi-square test, $p = 0.33$). These results indicate that although epithelial CD25/IL-2 signaling is not needed for epithelial migration and wound closure, it is important for the epithelial barrier function.

3.8 Comparison of CD25KO vs. CD25 $^{\Delta/\Delta CEpi}$ transcriptome changes in the corneal epithelium

In addition to exhibiting autoimmunity, the CD25KO mice also have decreased IL-2 signaling in the cornea. By contrast, the CD25$^{\Delta/\Delta CEpi}$ mice lack only CD25/IL-2 signaling in the corneal epithelium. To identify which DEGs result from immune cell changes or to IL-2 signaling in the cornea, we performed bulk RNA sequencing in the cornea epithelium of CD25$^{\Delta/\Delta CEpi}$ mice and compared their transcriptome to both CD25 and WT corneas. Fig. 8A shows that 246 genes were differentially modulated between CD25KO and CD25$^{\Delta/\Delta CEpi}$ (174 up and 72 down, Supplemental File 4). Since our purpose was to identify the common pathways (and not only DEGs) between these two groups, we used a subtraction approach. First, we compared CD25$^{\Delta/\Delta CEpi}$ to WT corneas. Then, we compared the unique and shared genes among the three comparisons (CD25KO/WT, CD25$^{\Delta/\Delta CEpi}$/WT

and CD25KO/CD25$^{\Delta/\Delta CEpi}$) using a Venn diagram. This subtractive approach allows us to identify which DEGs in the CD25/WT comparison are also seen in the CD25$^{\Delta/\Delta CEpi}$/WT mice and therefore identify common pathways that might be directly dependent on IL-2 signaling in the cornea. Venn diagram analysis showed 286 DEGs were shared between CD25KO and CD25$^{\Delta/\Delta CEpi}$ when compared to WT mice, while another 71 DEGs were present in CD25KO/WT and CD25/CD25$^{\Delta/\Delta CEpi}$ comparison (Fig. 8B-E).

Metascape analysis [60] of overrepresented pathways (irrespectively of being increased or decreased) was performed using the different sets of DEGs identified by the Venn diagram. The enriched pathways only in the CD25KO/WT comparison (412 genes) mapped to Amyotrophic lateral sclerosis (mmu05014), biosynthesis of amino acids (mmu01230), positive regulation of T cell receptor signaling pathway (GO:0050862), ribonucleotide catabolic process (GO:0050862), L-serine biosynthetic process (GO:0006564), regulation of cellular response to stress (GO:0080135), negative regulation of receptor signaling pathway via JAK-STAT (GO:0046426) among others (Fig. 8C). These pathways might indicate an effect of the immune system on the corneal epithelium. The shared 286 DEGs in CD25KO/WT and CD25KO/CD25$^{\Delta/\Delta CEpi}$/WT comparison might indicated the IL-2 direct signaling on the cornea: cytosolic ribosomal proteins (WP163); metabolism of RNA (R-MMU-8953854), regulation of signaling receptor activity (GO:0010469) and positive regulation of synaptic vesicle endocytosis (GO:1900244) (for others, see Fig 8D). Additional enriched pathways are shown in Fig. 8E and Fig. 8F as they related to the 88 and 71 unique DEGs according to the Venn Diagram (Fig. 8B). Taken together, these results suggest that disruption of IL-2 signaling in the cornea has a direct effect on the transcriptome of corneal epithelial cells. Future studies are needed to validate these findings at protein level.

4 Discussion

Our results confirmed that the corneal epithelium has all three chains of the IL-2R, both mRNA and protein levels. Transcriptome analysis revealed there are many altered pathways in the corneal epithelium of CD25KO mice. Interestingly, only female CD25KO mice displayed delayed wound healing after corneal debridement. But in agreement with this finding, conditional CD25KO mice also have a corneal phenotype that resembles that of spontaneous dry eye disease, despite normal lacrimal gland and meibomian gland architecture, comparable levels of VEGF-A in tears to C57BL/6J mice, and no alterations in the immune compartment, such as enlargement of the spleens or decreased Tregs. These findings indicate that corneal CD25 expression is necessary for maintaining corneal barrier function. Our transcriptome analysis also suggests that specific DEGs and pathways are modulated directly by IL-2/CD25 signaling in the cornea.

Our results show for the first time that corneal epithelium expresses mRNA and protein of all three IL-2R chains, suggesting the possibility of a functional receptor and a specific IL-2 signaling in the corneal epithelium. Using digital PCR, we assessed copy number/ng of all three IL-2R chains, not only in tissue biopsies, but also in cultured corneal epithelial cells. We further performed the *in vitro* experiments using cultured cells to confirm that corneal epithelial cells express all three mRNAs, since *in vivo* corneal epithelial tissues contain immune cell-derived RNA in addition to corneal epithelial cell RNA. We acknowledge

that human and mouse corneal epithelial cell culture changes corneal epithelial cell gene expression profiles. While corneal epithelial cells begin to undergo terminal differentiation and cease proliferating in vitro between 12-14 days, terminal differentiation is typically initiated by placing confluent cells in differentiation media with serum containing high calcium and placing cells at an air-liquid interface--conditions that stimulate cells to stratify and differentiate to form a barrier [80]. Here we used primary mouse and human corneal epithelial cells in a short-term culture grown in epithelial cell proliferation media. These conditions have been used in hundreds of studies that have contributed to our knowledge of how these epithelial cells function *in vitro* and *in vivo.* Using corneal epithelial tissue directly from the mouse or human cornea to assess gene expression and/or reducing the time corneal epithelial cells obtained from tissues are in culture may reduce gene expression changes in the corneal epithelial cells due to cell culture but increase the possibility of contamination of cultures by resident immune cells.

We found that CD25KO female mice healed slower than WT (irrespectively of sex) and CD25KO male mice. The CD25KO mice has been used extensively to investigate the consequences of lack of Tregs and activated effector T cells, has been used as a model of liver and lacrimal gland (and salivary) autoimmunity by many groups, including ours [28-30, 32-34, 36, 81-84]. In our previous studies, we found no sex differences regarding total lacrimal gland infiltration and corneal axon intraepithelial density [34, 36]. Since Pham and colleagues showed that corneal wound healing after corneal debridement is semi-dependent on corneal innervation [85], and our corneal nerves studies showed no sex effect on corneal innervation in a study that evaluated 50 male and 54 female CD25KO mice [36], we did not anticipate finding the CD25KO female mice would heal slower than CD25KO male mice (Fig. 4). Biological sex has been considered an important factor in cutaneous and dermal wound healing [86, 87]. It has been shown that cutaneous wounds heal faster in females than in males, while mucosal wounds heal faster in males [86, 87]. In corneal epithelial wound healing, the role of sex as a biological variable is influenced by the strain of mice (C57BL/6 or Balb/c) animal model (rabbit, dogs), and also type of injury (alkali burn, corneal debridement) and how the corneal debridement was made (using blade or a rotating bur) [85, 88-90]. A retrospective study recently investigated if there is a sex difference in corneal epithelial wound healing in persistent epithelial corneal defects in human subjects. The study concluded that women had greater epithelial healing time than men of the same age and similar treatment plans [91]. It is well established that female sex is a risk factor for dry eye, where corneal barrier disruption (as seen in both CD25KO and $CD25^{\Delta/\Delta CEpi}$ before and after injury) is a clinical hallmark. Future studies are needed to investigate the role of female sex in the CD25KO mice after corneal debridement and identify sex-specific changes in the transcriptome.

IPA analysis of the DEGs between wild-type and CD25KO mice predicted signal transducer and activator of transcription signal transduction (STAT)3 activation in the corneal epithelium in the female CD25KO mice. In T cells, IL-2 transduction activates Janus family kinase (JAK)1 and JAK3, followed by phosphorylation of STAT5 [92], while in intestinal epithelial cell lines, IL-2 stimulates JAK3 and STAT3 [23, 24]. In T cells, IL-2 also activates other signaling pathways, such as mitogen-activated protein kinase (MAPK), protein kinase B (AKT), phosphoinositide 3-kinase (Pi3K), and mammalian target of rapamycin (mTOR)

[93]. JAK2/STAT1 signaling has been implicated in corneal epithelial cell responses to LPS [94]. Inhibition of STAT3 signaling reduces inflammation caused by allergic conjunctivitis [95], and dry eye disease [96], while inhibition of JAK1/JAK3 decreases alkali burn injury-related inflammation [97]. On the other hand, STAT5 activation has been implicated in speeding cornea wound healing closure *in vitro* by mediating the migration of cells [98]. In certain epithelia, IL-2 signaling through IL-2R modulates epithelial renewal, wound healing, and apoptosis in a dose-dependent manner [16, 17, 23, 24]. In intestine cell lines, some of these functions are mediated by the phosphorylation of JAK3 and STAT3 [23, 24]. The activation of JAK/STAT and downstream pathways by IL-2/IL-2R signaling in corneal epithelial cells in homeostasis and non-inflamed conditions is unknown and we will further pursue this in a follow-up study.

Conditional deletion of CD25 in the corneal epithelium using the Cre-lox system led to a spontaneous dry eye phenotype with altered corneal barrier function and normal lacrimal gland function *in vivo* that was present only in female mice. This is the first report that shows that IL-2 signaling participates in cornea barrier function *in vivo.* Interestingly, these mice have normal ZO-1 distribution and epithelial thickness. It is possible that other tight junction proteins (such as claudin and occludin) might have subtle alterations that will require more advancing imaging techniques such as electron microscopy studies, which are beyond the scope of this initial report.

Mice do not blink very often; reports have suggested 1-2 blinks/minute in unstimulated eyes [99], so we did not use tear break-up time as a parameter in our study. Instead, we used VEGF concentration measurement in tears as a surrogate lacrimal gland function, which was within the normal range in CD25$^{\Delta/\Delta CEpi}$ mice, but it was decreased in the CD25KO mice. This is also in line with normal lacrimal gland architecture and no inflammation in the CD25$^{\Delta/\Delta CEpi}$ mice, in clear contrast to CD25KO mice that has atrophied glands and severe immune infiltration. Our findings regarding VEGF-A levels in tears in this study agree with our published results using aged mice, which have spontaneous dry eye, increased tear volume and increased concentration of inflammatory cytokines and immunoglobulins [46, 62, 100] in addition to lower VEGF-A concentration levels compared to young mice. While VEGF-A is involved in neovascularization [101], low levels of VEGF-A are present in tears of normal subjects [102]. Because VEGF-A is also neurotrophic [103, 104], it is possible that VEGF-A in tears might contribute to the preservation of corneal nerves. In support of this, we published that CD25KO mice have decreased corneal sensitivity and decreased axon density [36] and patients that received anti-VEGF therapy also show decreased corneal sensitivity and anatomical nerve differences compared to subjects that received no injections [105].

Our results with the CD25$^{\Delta/\Delta CEpi}$ mice indicate that CD25/IL-2 epithelial signaling is critical for apical corneal barrier maintenance, not migration of epithelial cells to close debridement wounds. This is consistent with the presence of CD25 in the suprabasal and wing layers of the cornea and its absence in the basal cell layer [106]. Yet, deleting CD25 systemically in all tissues leads to both barrier defects and delays in epithelial wound closure in female mice. These data taken together suggest that the lack of expression of CD25 in immune cells is responsible for the slower wound closure seen in female mice and also

point to differences in immune responses underlying the increased frequency of dry eye disease in women [107, 108]. We previously showed that CD25 expression decreases during desiccating stress and that desiccating-stress-induced MMP-9 cleaves CD25 from the ocular surface [20]. Therefore, the lack of CD25/IL-2 signaling might be part of the vicious circle of dry eye disease. This is supported by spontaneous dry eye alterations in the CD25$^{\Delta/\Delta CEpi}$ mice.

The transcriptome analysis of corneal epithelial cells showed many differentially modulated pathways between CD25KO and WT mice. However, these changes include indirect and direct effects of IL-2 on the corneal epithelium. We attempted to identify specific pathways that are modulated in both CD25KO/WT and CD25$^{\Delta/\Delta CEpi}$/WT mice using a Venn diagram and subtracting the changes in the CD25KO/CD25$^{\Delta/\Delta CEpi}$. We identified for the first time that IL-2/CD25 signaling might modulate cytoplasmic ribosomal proteins and RNA metabolism, cholesterol and keratan biosynthesis, intracellular cholesterol transport and many other metabolic processes, including regulation of ATP and regulation of synaptic vesicle endocytosis. These pathways will need validation at protein level either using primary cultured epithelial cells or epithelial cells collected from live animals. They might be better investigated in cultured systems where epithelial cells can be isolated from the immune cells.

The eye is a delicate organ that has strong immune mechanisms that decrease inflammation and prevent bystander tissue scarring, which could cause a loss of transparency. One of the mechanisms responsible for the immune privilege of the eye is the expression of Fas-ligand in non-lymphoid structures, like the cornea, iris, and retina [109, 110]. Cells that express Fas will undergo apoptosis after interaction with Fas-ligand, initiating caspase 8-mediated apoptosis [111], which is critical for tolerance induction [109]. We previously published that CD25 might be a functional receptor in the corneal epithelium, as IL-2 subconjunctival injections increased Fas-ligand in the cornea and conjunctiva epithelium [20], in agreement with the literature that IL-2 stimulates the expression of Fas-ligand [112]. In homeostasis, constant basal stimulation of Fas-ligand in the corneal epithelium may come from tears, since low levels of IL-2 are detectable in the tears of healthy subjects [68-73]. It is plausible to speculate that a low, constant IL-2/CD25 signaling might be present in the cornea in normal conditions providing homeostatic signals to the cornea epithelium.

Taken together, we showed that corneal epithelia express all three chains of the IL-2R and our in vivo studies using a conditional deletion of CD25 only in the corneal epithelia suggest that there might be an IL-2/CD25 signaling that is important for corneal barrier function in naive conditions. Future studies are needed to delineate and investigate the effects of CD25/IL-2 signaling in other corneal pathologies including diseases such as dry eye.

Supplementary Material

Refer to Web version on PubMed Central for supplementary material.

Acknowledgments

This work was supported by the Research to Prevent Blindness Stein Innovation Award (CSdP), Lions Foundation for Sight (KKS), National Institutes of Health/National Eye Institute R01EY030447 (CSdP), EY002520 Center Core Grant for Vision Research (Department of Ophthalmology at Baylor College of Medicine), NEI Training Grant in Vision Sciences T32 EY007001 (KKS); Research to Prevent Blindness (Dept. of Ophthalmology), The Hamill Foundation, The Sid Richardson Foundation, Baylor College of Medicine Pathology Core (NCI P30CA125123). This project was supported by the Cytometry and Cell Sorting Core at Baylor College of Medicine with funding from the NIH (CA125123 and RR024574) from a CPRIT Core Facility Support Award (RP180672), and the expert assistance of Joel M. Sederstrom. The funders had no role in the design and conduct of the study; collection, management, analysis, and interpretation of the data; preparation, review, or approval of the manuscript; and decision to submit the manuscript for publication.) Mary Ann Stepp is funded by NIH/NEI EY08512.

We acknowledge the contribution of Leiqi Zhang with the management of the mice colony and Sarah Amra for the histology preparation. We also thank Elizabeth Zuniga-Sanchez for sharing the Ai14 mice.

Data availability statement.

Uncropped western blot images are provided as Supplemental Figures. Further inquiries can be directed to the corresponding author. The datasets for this study can be found in the GEO repository (GSE ID pending).

References

[1]. Stepp MA, Tadvalkar G, Hakh R, Pal-Ghosh S. Corneal epithelial cells function as surrogate Schwann cells for their sensory nerves. Glia. 2017;65:851–63. [PubMed: 27878997]

[2]. Chiambaretta Fdr, Lc Blanchon, Bnd Rabier, Kao WWY, Liu JJ, Dastugue B, et al. Regulation of Corneal Keratin-12 Gene Expression by the Human Krüppel-like Transcription Factor 6. Investigative Ophthalmology & Visual Science. 2002;43:3422–9. [PubMed: 12407152]

[3]. Coulson-Thomas VJ, Chang SH, Yeh LK, Coulson-Thomas YM, Yamaguchi Y, Esko J, et al. Loss of corneal epithelial heparan sulfate leads to corneal degeneration and impaired wound healing. Invest Ophthalmol Vis Sci. 2015;56:3004–14. [PubMed: 26024086]

[4]. Kasetti RB, Gaddipati S, Tian S, Xue L, Kao WWY, Lu Q, et al. Study of corneal epithelial progenitor origin and the Yap1 requirement using keratin 12 lineage tracing transgenic mice. Scientific reports. 2016;6:35202-. [PubMed: 27734924]

[5]. Liu CY, Zhu G, Converse R, Kao CWC, Nakamura H, Tseng SCG, et al. Characterization and chromosomal localization of the cornea-specific murine keratin gene Krt1.12. JBiolChem. 1994;260:24627–36.

[6]. Liu CY, Zhu G, Westerhausen-Larson A, Converse R, Kao CW, Sun TT, et al. Cornea-specific expression of K12 keratin during mouse development. Current eye research. 1993;12:963–74. [PubMed: 7508359]

[7]. Taniguchi T, Minami Y. The IL-2/IL-2 receptor system: a current overview. Cell. 1993;73:5–8. [PubMed: 8462103]

[8]. Povoleri GA, Scotta C, Nova-Lamperti EA, John S, Lombardi G, Afzali B. Thymic versus induced regulatory T cells - who regulates the regulators? Frontiers in immunology. 2013;4:169. [PubMed: 23818888]

[9]. Fan MY, Low JS, Tanimine N, Finn KK, Priyadharshini B, Germana SK, et al. Differential Roles of IL-2 Signaling in Developing versus Mature Tregs. Cell reports. 2018;25:1204–13.e4. [PubMed: 30380412]

[10]. Dahlman-Hoglund A, Ahlstedt S, Hanson LA, Dahlgren U, Telemo E. Different expression of IL-2 receptor alpha-chain on a lamina propria T cell population and goblet cells in rats orally tolerized or sensitized to ovalbumin (OA) after colonization with an OA-producing Escherichia coli. Clinical and experimental immunology. 1996;106:534–40. [PubMed: 8973624]

[11]. Coll J, Tomas S, Vilella R, Corominas J. Interleukin-2 receptor expression in salivary glands of patients with Sjogren's syndrome. The Journal of rheumatology. 1995;22:1488–91. [PubMed: 7473471]

[12]. Spadaro A, Riccieri V, Benfari G, Scillone M, Taccari E. Soluble interleukin-2 receptor in Sjogren's syndrome: relation to main serum immunological and immunohistochemical parameters. ClinRheumatol. 2001;20:319–23.

[13]. Tomas S, Coll J, Palazon X. Soluble interleukin-2 receptor in primary and secondary Sjogren's syndrome. BrJRheumatol. 1997;36:194–7.

[14]. Wang S, Zhang Z-X, Yin Z, Liu W, Garcia B, Huang X, et al. Anti-IL-2 receptor antibody decreases cytokine-induced apoptosis of human renal tubular epithelial cells (TEC). Nephrology Dialysis Transplantation. 2010;26:2144–53.

[15]. Plaisance S, Rubinstein E, Alileche A, Sahraoui Y, Krief P, Augery-Bourget Y, et al. Expression of the interleukin-2 receptor on human fibroblasts and its biological significance. International immunology. 1992;4:739–46. [PubMed: 1379826]

[16]. Ciacci C, Mahida YR, Dignass A, Koizumi M, Podolsky DK. Functional interleukin-2 receptors on intestinal epithelial cells. JClinInvest. 1993;92:527–32.

[17]. Dignass AU, Podolsky DK. Interleukin 2 modulates intestinal epithelial cell function in vitro. ExpCell Res. 1996;225:422–9.

[18]. Lapchak PA, Araujo DM, Quirion R, Beaudet A. Immunoautoradiographic localization of interleukin 2-like immunoreactivity and interleukin 2 receptors (Tac antigen-like immunoreactivity) in the rat brain. Neuroscience. 1991;44:173–84. [PubMed: 1770995]

[19]. Lesur O, Arsalane K, Bérard J, Mukuna JP, de Brum-Fernandes AJ, Lane D, et al. Functional IL-2 receptors are expressed by rat lung type II epithelial cells. Am J Physiol. 1997;273:L495–503. [PubMed: 9316482]

[20]. de Paiva CS, Yoon KC, Pangelinan SB, Pham S, Puthenparambil LM, Chuang EY, et al. Cleavage of functional IL-2 receptor alpha chain (CD25) from murine corneal and conjunctival epithelia by MMP-9. JInflamm(Lond). 2009;6:31. [PubMed: 19878594]

[21]. Hendricks RL, Malek TR, Yue BY. Expression of a p55 interleukin-2 receptor-like molecule on corneal epithelial cells. Reg Immunol. 1990;3:29–34. [PubMed: 2223555]

[22]. Zhang Y, Xie J, Qian L, Schechter JE, Mircheff AK. IL-2 immunoreactive proteins in lacrimal acinar cells. Advances in experimental medicine and biology. 2002;506:795–9. [PubMed: 12613994]

[23]. Kumar N, Mishra J, Narang VS, Waters CM. Janus kinase 3 regulates interleukin 2-induced mucosal wound repair through tyrosine phosphorylation of villin. The Journal of biological chemistry. 2007;282:30341–5. [PubMed: 17537734]

[24]. Mishra J, Waters CM, Kumar N. Molecular mechanism of interleukin-2-induced mucosal homeostasis. American journal of physiology Cell physiology. 2012;302:C735–47. [PubMed: 22116305]

[25]. Dieckmann D, Bruett CH, Ploettner H, Lutz MB, Schuler G. Human CD4(+)CD25(+) regulatory, contact-dependent T cells induce interleukin 10-producing, contact-independent type 1-like regulatory T cells [corrected]. JExpMed. 2002;196:247–53.

[26]. Skelsey ME, Mayhew E, Niederkorn JY. CD25+, interleukin-10-producing CD4+ T cells are required for suppressor cell production and immune privilege in the anterior chamber of the eye. Immunology. 2003;110:18–29. [PubMed: 12941137]

[27]. Foussat A, Cottrez F, Brun V, Fournier N, Breittmayer JP, Groux H. A comparative study between T regulatory type 1 and CD4+CD25+ T cells in the control of inflammation. JImmunol. 2003;171:5018–26. [PubMed: 14607898]

[28]. Willerford DM CJ, Ferry JA, Davidson L, Ma A, Alt FW. Interleukin-2 receptor alpha chain regulates the size and content of the peripheral lymphoid compartment. Immunity. 1995;3:521–30. [PubMed: 7584142]

[29]. Sharma R, Zheng L, Deshmukh US, Jarjour WN, Sung SS, Fu SM, et al. A regulatory T cell-dependent novel function of CD25 (IL-2Ralpha) controlling memory CD8(+) T cell homeostasis. Journal of immunology. 2007;178:1251–5.

[30]. Sharma R, Zheng L, Guo X, Fu SM, Ju ST, Jarjour WN. Novel animal models for Sjogren's syndrome: expression and transfer of salivary gland dysfunction from regulatory T cell-deficient mice. Journal of autoimmunity. 2006;27:289–96. [PubMed: 17207605]

[31]. Sharma R, Bagavant H, Jarjour WN, Sung SS, Ju ST. The role of Fas in the immune system biology of IL-2R alpha knockout mice: interplay among regulatory T cells, inflammation, hemopoiesis, and apoptosis. JImmunol. 2005;175:1965–73. [PubMed: 16034141]

[32]. de Paiva CS, Hwang CS, Pitcher JD III, Pangelinan SB, Rahimy E, Chen W, et al. Age-related T-cell cytokine profile parallels corneal disease severity in Sjogren's syndrome-like keratoconjunctivitis sicca in CD25KO mice. Rheumatology. 2010;49:246–58. [PubMed: 20007286]

[33]. Zaheer M, Wang C, Bian F, Yu Z, Hernandez H, de Souza RG, et al. Protective role of commensal bacteria in Sjogren Syndrome. Journal of autoimmunity. 2018:45–56.

[34]. Rahimy E, Pitcher JD III, Pangelinan SB, Chen W, Farley WJ, Niederkorn JY, et al. Spontaneous autoimmune dacryoadenitis in aged CD25KO mice. Am J Pathol. 2010; 177:744–53 Epub 2010 Jun 21. [PubMed: 20566743]

[35]. Chinen T, Kannan AK, Levine AG, Fan X, Klein U, Zheng Y, et al. An essential role for the IL-2 receptor in Treg cell function. Nature immunology. 2016;17:1322–33. [PubMed: 27595233]

[36]. Stepp MA, Pal-Ghosh S, Tadvalkar G, Williams AR, Pflugfelder SC, de Paiva CS. Reduced Corneal Innervation in the CD25 Null Model of Sjogren Syndrome. International journal of molecular sciences. 2018; 19:3821 [PubMed: 30513621]

[37]. Chikama T, Hayashi Y, Liu CY, Terai N, Terai K, Kao CW, et al. Characterization of tetracycline-inducible bitransgenic Krt12rtTA/+/tet-O-LacZ mice. Invest Ophthalmol Vis Sci. 2005;46:1966–72. [PubMed: 15914610]

[38]. Perl AK, Wert SE, Nagy A, Lobe CG, Whitsett JA. Early restriction of peripheral and proximal cell lineages during formation of the lung. Proceedings of the National Academy of Sciences of the United States of America. 2002;99:10482–7. [PubMed: 12145322]

[39]. Toomer KH, Lui JB, Altman NH, Ban Y, Chen X, Malek TR. Essential and non-overlapping IL-2Rα-dependent processes for thymic development and peripheral homeostasis of regulatory T cells. Nature communications. 2019; 10:1037.

[40]. de Paiva CS, Villarreal AL, Corrales RM, Rahman HT, Chang VY, Farley WJ, et al. Dry Eye-Induced Conjunctival Epithelial Squamous Metaplasia Is Modulated by Interferon-{gamma}. Invest Ophthalmol Vis Sci. 2007;48:2553–60. [PubMed: 17525184]

[41]. Li DQ, Chen Z, Song XJ, de Paiva CS, Kim HS, Pflugfelder SC. Partial enrichment of a population of human limbal epithelial cells with putative stem cell properties based on collagen type IV adhesiveness. ExpEye Res. 2005;80:581–90.

[42]. Hu J, Gao N, Zhang Y, Chen X, Li J, Bian F, et al. IL-33/ST2/IL-9/IL-9R signaling disrupts ocular surface barrier in allergic inflammation. Mucosal immunology. 2020;13:919–30. [PubMed: 32358573]

[43]. Schaefer L, Hernandez H, Coats RA, Yu Z, Pflugfelder SC, Britton RA, et al. Gut-derived butyrate suppresses ocular surface inflammation. Scientific reports. 2022; 12:4512. [PubMed: 35296712]

[44]. Pal-Ghosh S, Pajoohesh-Ganji A, Tadvalkar G, Kyne BM, Guo X, Zieske JD, et al. Topical Mitomycin-C enhances subbasal nerve regeneration and reduces erosion frequency in the debridement wounded mouse cornea. Exp Eye Res. 2016;146:361–9. [PubMed: 26332224]

[45]. Trujillo-Vargas CM, Mauk KE, Hernandez H, de Souza RG, Yu Z, Galletti JG, et al. Immune phenotype of the CD4+ T cells in the aged lymphoid organs and lacrimal glands. GeroScience. 2022;44:2105–28. [PubMed: 35279788]

[46]. Galletti JG, Scholand KK, Trujillo-Vargas CM, Yu Z, Mauduit O, Delcroix V, et al. Ectopic lymphoid structures in the aged lacrimal glands. Clinical immunology. 2023;248:109251. [PubMed: 36740002]

[47]. Yu Z, Joy S, Mi T, Yazdanpanah G, Burgess K, de Paiva CS. New, potent, small molecule agonists of tyrosine kinase receptors attenuate dry eye disease. Front Med (Lausanne). 2022;9:937142. [PubMed: 36091713]

[48]. Yu Z, Li J, Govindarajan G, Hamm-Alvarez SF, Alam J, Li DQ, et al. Cathepsin S is a novel target for age-related dry eye. Exp Eye Res. 2021;214:108895. [PubMed: 34910926]

[49]. Martin M. Cutadapt removes adapter sequences from high-throughput sequencing reads. EMBnetjournal. 2011;17:10–2.

[50]. Dobin A, Davis CA, Schlesinger F, Drenkow J, Zaleski C, Jha S, et al. STAR: ultrafast universal RNA-seq aligner. Bioinformatics. 2013;29:15–21. [PubMed: 23104886]

[51]. Anders S, Pyl PT, Huber W. HTSeq—a Python framework to work with high-throughput sequencing data. Bioinformatics. 2015;31:166–9. [PubMed: 25260700]

[52]. Love MI, Huber W, Anders S. Moderated estimation of fold change and dispersion for RNA-seq data with DESeq2. Genome Biology. 2014;15:550. [PubMed: 25516281]

[53]. Wang L, Wang S, Li W. RSeQC: quality control of RNA-seq experiments. Bioinformatics. 2012;28:2184–5. [PubMed: 22743226]

[54]. Alexa A JR topGO: Enrichment Analysis for Gene Ontology. R package version 1381. 2019.

[55]. Mitchell AL, Attwood TK, Babbitt PC, Blum M, Bork P, Bridge A, et al. InterPro in 2019: improving coverage, classification and access to protein sequence annotations. Nucleic acids research. 2019;47:D351–D60. [PubMed: 30398656]

[56]. Geer LY, Marchler-Bauer A, Geer RC, Han L, He J, He S, et al. The NCBI BioSystems database. Nucleic acids research. 2010;38:D492–6. [PubMed: 19854944]

[57]. Subramanian A, Tamayo P, Mootha VK, Mukherjee S, Ebert BL, Gillette MA, et al. Gene set enrichment analysis: a knowledge-based approach for interpreting genome-wide expression profiles. Proceedings of the National Academy of Sciences of the United States of America. 2005;102:15545–50. [PubMed: 16199517]

[58]. Fabregat A, Jupe S, Matthews L, Sidiropoulos K, Gillespie M, Garapati P, et al. The Reactome Pathway Knowledgebase. Nucleic acids research. 2018;46:D649–d55. [PubMed: 29145629]

[59]. Slenter DN, Kutmon M, Hanspers K, Riutta A, Windsor J, Nunes N, et al. WikiPathways: a multifaceted pathway database bridging metabolomics to other omics research. Nucleic acids research. 2018;46:D661–d7. [PubMed: 29136241]

[60]. Zhou Y, Zhou B, Pache L, Chang M, Khodabakhshi AH, Tanaseichuk O, et al. Metascape provides a biologist-oriented resource for the analysis of systems-level datasets. Nature communications. 2019;10:1523.

[61]. Oliveros JC. Venny. An interactive tool for comparing lists with Venn's diagrams. https://bioinfogpcnbcsices/tools/venny/indexhtml. 2007.

[62]. de Souza RG, Yu Z, Hernandez H, Trujillo-Vargas CM, Lee A, Mauk KE, et al. Modulation of Oxidative Stress and Inflammation in the Aged Lacrimal Gland. The American journal of pathology. 2021;191:294–308. [PubMed: 33159886]

[63]. Moore QL, de Paiva CS, Pflugfelder SC. Effects of dry eye therapies on environmentally induced ocular surface disease. Am J Ophthalmol. 2015;160:135–42. [PubMed: 25868759]

[64]. Kim HS, Jun SX, de Paiva CS, Chen Z, Pflugfelder SC, Li DQ. Phenotypic characterization of human corneal epithelial cells expanded ex vivo from limbal explant and single cell cultures. ExpEye Res. 2004;79:41–9.

[65]. Tukler Henriksson J, Coursey TG, Corry DB, De Paiva CS, Pflugfelder SC. IL-13 Stimulates Proliferation and Expression of Mucin and Immunomodulatory Genes in Cultured Conjunctival Goblet Cells. Invest Ophthalmol Vis Sci. 2015;56:4186–97. [PubMed: 26132778]

[66]. Coursey TG, Henriksson JT, Barbosa FL, de Paiva CS, Pflugfelder SC. Interferon-gamma-Induced Unfolded Protein Response in Conjunctival Goblet Cells as a Cause of Mucin Deficiency in Sjogren Syndrome. The American journal of pathology. 2016;186:1547–58. [PubMed: 27085137]

[67]. Lee MJ, Ko AY, Ko JH, Lee HJ, Kim MK, Wee WR, et al. Mesenchymal stem/stromal cells protect the ocular surface by suppressing inflammation in an experimental dry eye. Mol Ther. 2015;23:139–46. [PubMed: 25152016]

[68]. Roda M, Corazza I, Bacchi Reggiani ML, Pellegrini M, Taroni L, Giannaccare G, et al. Dry Eye Disease and Tear Cytokine Levels-A Meta-Analysis. International journal of molecular sciences. 2020;21.

[69]. Massingale ML, Li X, Vallabhajosyula M, Chen D, Wei Y, Asbell PA. Analysis of inflammatory cytokines in the tears of dry eye patients. Cornea. 2009;28:1023–7. [PubMed: 19724208]

[70]. Lee SY, Han SJ, Nam SM, Yoon SC, Ahn JM, Kim TI, et al. Analysis of tear cytokines and clinical correlations in Sjögren syndrome dry eye patients and non-Sjögren syndrome dry eye patients. Am J Ophthalmol. 2013;156:247–53.e1. [PubMed: 23752063]

[71]. Chen X, Aqrawi LA, Utheim TP, Tashbayev B, Utheim ØA, Reppe S, et al. Elevated cytokine levels in tears and saliva of patients with primary Sjögren's syndrome correlate with clinical ocular and oral manifestations. Scientific reports. 2019;9:7319. [PubMed: 31086200]

[72]. Nair S, Vanathi M, Mahapatra M, Seth T, Kaur J, Velpandian T, et al. Tear inflammatory mediators and protein in eyes of post allogenic hematopoeitic stem cell transplant patients. Ocul Surf. 2018;16:352–67. [PubMed: 29723628]

[73]. Cocho L, Fernández I, Calonge M, Martínez V, González-García MJ, Caballero D, et al. Biomarkers in Ocular Chronic Graft Versus Host Disease: Tear Cytokine- and Chemokine-Based Predictive Model. Invest Ophthalmol Vis Sci. 2016;57:746–58. [PubMed: 26927568]

[74]. Foxwell B, Taylor D, Ryffel B. Comparison of the structure of the murine interleukin 2 (IL 2) receptor on cytotoxic and helper T cell lines by chemical cross-linking of 125I-labeled IL 2. European journal of immunology. 1988;18:1515–9. [PubMed: 2973414]

[75]. Shi K, Yin Q, Tang X, Yu X, Zheng S, Shentu X. Necroptosis contributes to airborne particulate matter-induced ocular surface injury. Toxicology. 2022;470:153140. [PubMed: 35247514]

[76]. Sonawane S, Khanolkar V, Namavari A, Chaudhary S, Gandhi S, Tibrewal S, et al. Ocular surface extracellular DNA and nuclease activity imbalance: a new paradigm for inflammation in dry eye disease. Invest OphthalmolVisSci. 2012;53:8253–63.

[77]. Hirano T Long-term depression and other synaptic plasticity in the cerebellum. Proc Jpn Acad Ser B Phys Biol Sci. 2013;89:183–95.

[78]. de Paiva CS, Corrales RM, Villarreal AL, Farley W, Li DQ, Stern ME, et al. Apical corneal barrier disruption in experimental murine dry eye is abrogated by methylprednisolone and doxycycline. Invest Ophthalmol Vis Sci. 2006;47:2847–56. [PubMed: 16799024]

[79]. Beardsley RM, de Paiva CS, Power DF, Pflugfelder SC. Desiccating stress decreases apical corneal epithelial cell size--modulation by the metalloproteinase inhibitor doxycycline. Cornea. 2008;27:935–40. [PubMed: 18724157]

[80]. Ma P, Bian F, Wang Z, Zheng X, Chotikavanich S, Pflugfelder SC, et al. Human corneal epithelium-derived thymic stromal lymphopoietin links the innate and adaptive immune responses via TLRs and Th2 cytokines. Invest OphthalmolVisSci. 2009;50:2702–9.

[81]. Sharma R, Jarjour WN, Zheng L, Gaskin F, Fu SM, Ju ST. Large functional repertoire of regulatory T-cell suppressible autoimmune T cells in scurfy mice. Journal of autoimmunity. 2007;29:10–9. [PubMed: 17521882]

[82]. Pelegrino FS, Volpe EA, Gandhi NB, Li DQ, Pflugfelder SC, de Paiva CS. Deletion of interferon-gamma delays onset and severity of dacryoadenitis in CD25KO mice. Arthritis Res Ther. 2012;14:R234. [PubMed: 23116218]

[83]. Yang W, Yao Y, Yang YQ, Lu FT, Li L, Wang YH, et al. Differential modulation by IL-17A of Cholangitis versus Colitis in IL-2Ralpha deleted mice. PLoS One. 2014;9:e105351. [PubMed: 25133396]

[84]. Wakabayashi K, Lian ZX, Moritoki Y, Lan RY, Tsuneyama K, Chuang YH, et al. IL-2 receptor alpha(−/−) mice and the development of primary biliary cirrhosis. Hepatology. 2006;44:1240–9. [PubMed: 17058261]

[85]. Pham TL, Kakazu A, He J, Bazan HEP. Mouse strains and sexual divergence in corneal iinnervation and nerve regeneration. Faseb j. 2019;33:4598–609. [PubMed: 30561223]

[86]. Ashcroft GS, Ashworth JJ. Potential role of estrogens in wound healing. Am J Clin Dermatol. 2003;4:737–43.

[87]. Ashcroft GS, Dodsworth J, van Boxtel E, Tarnuzzer RW, Horan MA, Schultz GS, et al. Estrogen accelerates cutaneous wound healing associated with an increase in TGF-beta1 levels. Nature medicine. 1997;3:1209–15.

[88]. Wang SB, Hu KM, Seamon KJ, Mani V, Chen Y, Gronert K. Estrogen negatively regulates epithelial wound healing and protective lipid mediator circuits in the cornea. Faseb j. 2012;26:1506–16. [PubMed: 22186873]

[89]. Moore PA. Diagnosis and management of chronic corneal epithelial defects (indolent corneal ulcerations). Clin Tech Small Anim Pract.2003;18:168–77. [PubMed: 14604091]

[90]. Tripathi R, Giuliano EA, Gafen HB, Gupta S, Martin LM, Sinha PR, et al. Is sex a biological variable in corneal wound healing? Exp Eye Res. 2019;187:107705. [PubMed: 31226339]

[91]. Coco G, Hamill KJ, Troughton LD, Kaye SB, Romano V. Risk factors for corneal epithelial wound healing: Can sex play a role? European journal of ophthalmology. 2022;32:2676–82. [PubMed: 34889141]

[92]. Ross SH, Cantrell DA. Signaling and Function of Interleukin-2 in T Lymphocytes. Annual review of immunology. 2018;36:411–33.

[93]. Powell JD, Pollizzi KN, Heikamp EB, Horton MR. Regulation of Immune Responses by mTOR. Annual Review of Immunology. 2012;30:39–68.

[94]. Roy S, Sun Y, Pearlman E. Interferon-gamma-induced MD-2 protein expression and lipopolysaccharide (LPS) responsiveness in corneal epithelial cells is mediated by Janus tyrosine kinase-2 activation and direct binding of STAT1 protein to the MD-2 promoter. The Journal of biological chemistry. 2011;286:23753–62. [PubMed: 21572044]

[95]. Guo C, Liu J, Hao P, Wang Y, Sui S, Li L, et al. The Potential Inhibitory Effects of miR-19b on Ocular Inflammation are Mediated Upstream of the JAK/STAT Pathway in a Murine Model of Allergic Conjunctivitis. Invest Ophthalmol Vis Sci. 2020;61:8.

[96]. Qu M, Qi X, Wang Q, Wan L, Li J, Li W, et al. Therapeutic Effects of STAT3 Inhibition on Experimental Murine Dry Eye. Invest Ophthalmol Vis Sci. 2019;60:3776–85. [PubMed: 31503282]

[97]. Sakimoto T, Ishimori A. Anti-inflammatory effect of topical administration of tofacitinib on corneal inflammation. Exp Eye Res. 2016;145:110–7. [PubMed: 26689752]

[98]. Ding J, Wirostko B, Sullivan DA. Human growth hormone promotes corneal epithelial cell migration in vitro. Cornea. 2015;34:686–92. [PubMed: 25782399]

[99]. Martinez J, Cunha LD, Park S, Yang M, Lu Q, Orchard R, et al. Noncanonical autophagy inhibits the autoinflammatory, lupus-like response to dying cells. Nature. 2016;533:115–9. [PubMed: 27096368]

[100]. Galletti JG, de Paiva CS. Age-related changes in ocular mucosal tolerance: Lessons learned from gut and respiratory tract immunity. Immunology. 2021.

[101]. Brown LF, Detmar M, Claffey K, Nagy JA, Feng D, Dvorak AM, et al. Vascular permeability factor/vascular endothelial growth factor: a multifunctional angiogenic cytokine. EXS. 1997;79:233–69. [PubMed: 9002222]

[102]. Vesaluoma M, Teppo AM, Grönhagen-Riska C, Tervo T. Release of TGF-beta 1 and VEGF in tears following photorefractive keratectomy. Current eye research. 1997;16:19–25. [PubMed: 9043819]

[103]. Góra-Kupilas K, Jośko J. The neuroprotective function of vascular endothelial growth factor (VEGF). Folia Neuropathol. 2005;43:31–9. [PubMed: 15827888]

[104]. Nishijima K, Ng YS, Zhong L, Bradley J, Schubert W, Jo N, et al. Vascular endothelial growth factor-A is a survival factor for retinal neurons and a critical neuroprotectant during the adaptive response to ischemic injury. The American journal of pathology. 2007;171:53–67. [PubMed: 17591953]

[105]. Goldhardt R, Batawi HIM, Rosenblatt M, Lollett IV, Park JJ, Galor A. Effect of Anti-Vascular Endothelial Growth Factor Therapy on Corneal Nerves. Cornea. 2019;38:559–64. [PubMed: 30933961]

[106]. Ljubimov AV, Saghizadeh M. Progress in corneal wound healing. Progress in retinal and eye research. 2015;49:17–45. [PubMed: 26197361]

[107]. Schaumberg DA, Dana R, Buring JE, Sullivan DA. Prevalence of dry eye disease among US men: estimates from the Physicians' Health Studies. Arch Ophthalmol. 2009;127:763–8. [PubMed: 19506195]

[108]. Schaumberg DA, Sullivan DA, Buring JE, Dana MR. Prevalence of dry eye syndrome among US women. Am J Ophthalmol. 2003;136:318–26. [PubMed: 12888056]

[109]. Griffith TS, Yu X, Herndon JM, Green DR, Ferguson TA. CD95-induced apoptosis of lymphocytes in an immune privileged site induces immunological tolerance. Immunity. 1996;5:7–16. [PubMed: 8758890]

[110]. Griffith TS, Brunner T, Fletcher SM, Green DR, Ferguson TA. Fas ligand-induced apoptosis as a mechanism of immune privilege. Science. 1995;270:1189–92. [PubMed: 7502042]

[111]. Jabs DA, Lee B, Whittum-Hudson J, Prendergast RA. The Role of Fas-Fas Ligand–Mediated Apoptosis in Autoimmune Lacrimal Gland Disease in MRL/MpJ Mice. Invest Ophthalmol Vis Sci. 2001;42:399–401. [PubMed: 11157873]

[112]. Refaeli Y, Van Parijs L, London CA, Tschopp J, Abbas AK. Biochemical mechanisms of IL-2-regulated Fas-mediated T cell apoptosis. Immunity. 1998;8:615–23. [PubMed: 9620682]

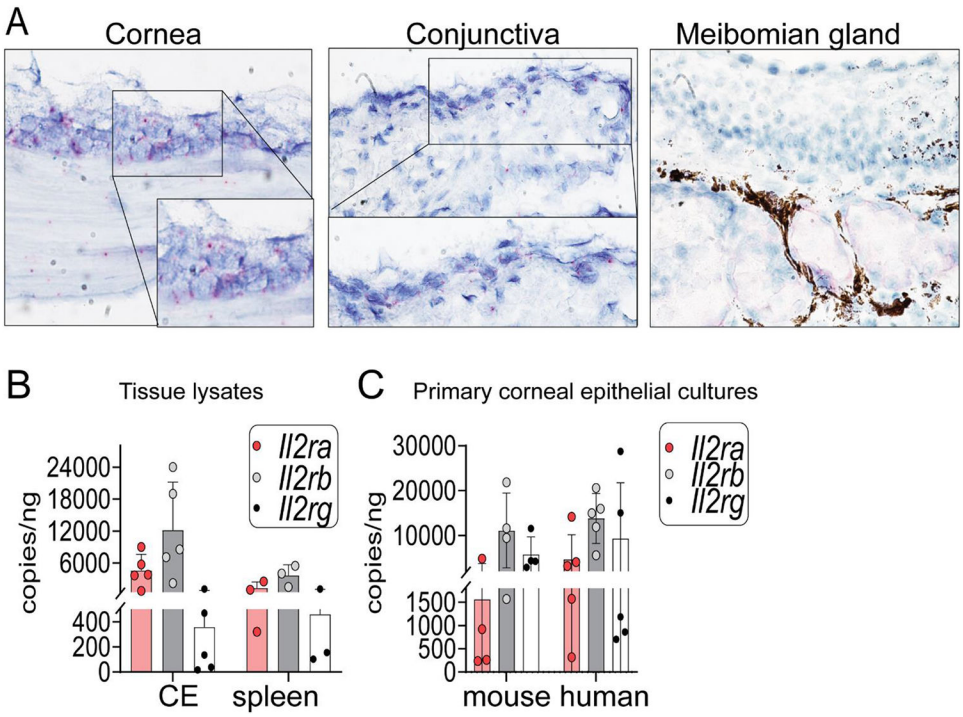

Fig. 1: CD25 mRNA is expressed in the cornea.

A. Representative RNA scope in-situ hybridization (pink-red) with hematoxylin counterstaining in frozen sections, n = 3.

B. Quantitative digital PCR was used to amplify cDNA prepared from wild-type C57BL/6 murine corneal epithelium (CE) and spleen lysates. Each data point represents tissue from one animal, n = 3-5. The number of transcripts detected was normalized to the concentration of DNA.

C. Quantitative digital PCR was used to amplify cDNA prepared from primary corneal epithelial cultures from either mouse or human corneas. The number of transcripts detected was normalized to the concentration of DNA.

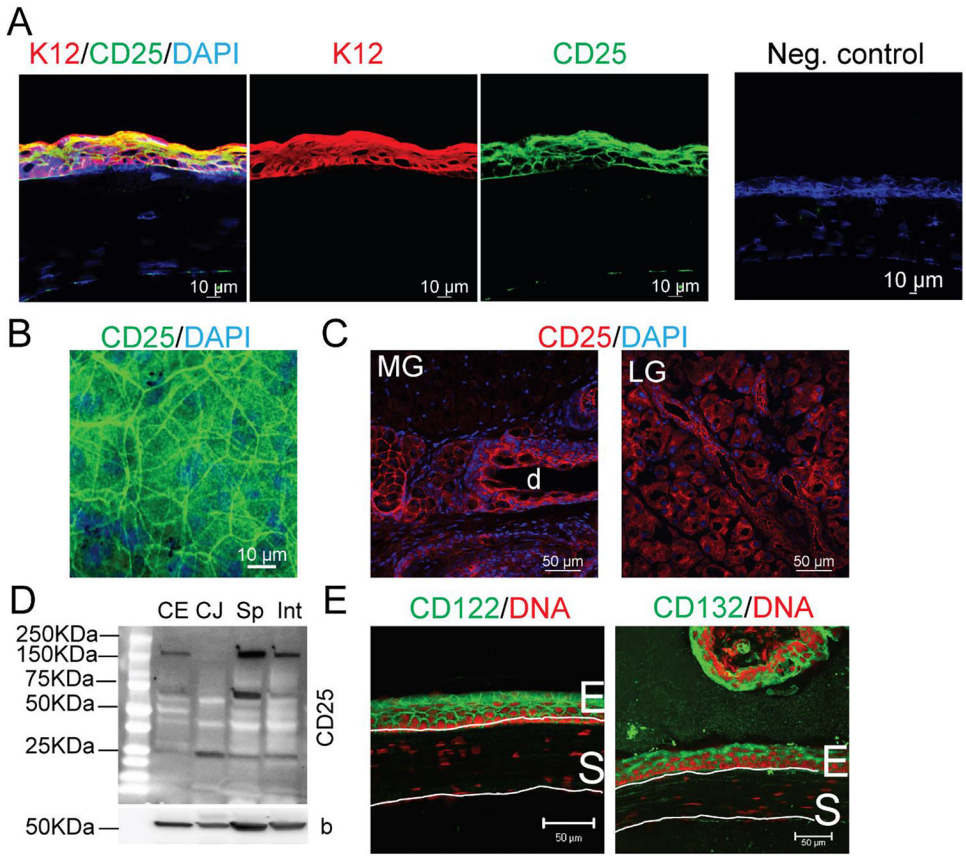

Fig. 2: All three chains of IL-2 receptor are expressed in the cornea.

A. Representative images of corneas stained with CD25 (green) and Krt12 (red) antibodies with Hoechst 33342 nuclear counterstaining (DNA, blue).

B. Representative images of laser confocal microscope Z stacks of whole-mount corneas stained with CD25 (green) with Hoechst 33342 nuclear counterstaining (blue).

C. Representative images of Meibomian gland (MG) and lacrimal gland (LG) stained with CD25 (red) antibody with Hoechst 33342 nuclear counterstaining (blue). d = duct.

D. Western blot image showing CD25 and β-actin (b) bands in corneal epithelium (CE), conjunctiva (CJ), spleen (Sp), and intestine (Int).

E. Representative images of murine corneas stained with CD122 or CD132 (green: IL-2Rβ and IL-2Rγ chains, respectively) with propidium iodide (red) nuclear counterstaining.

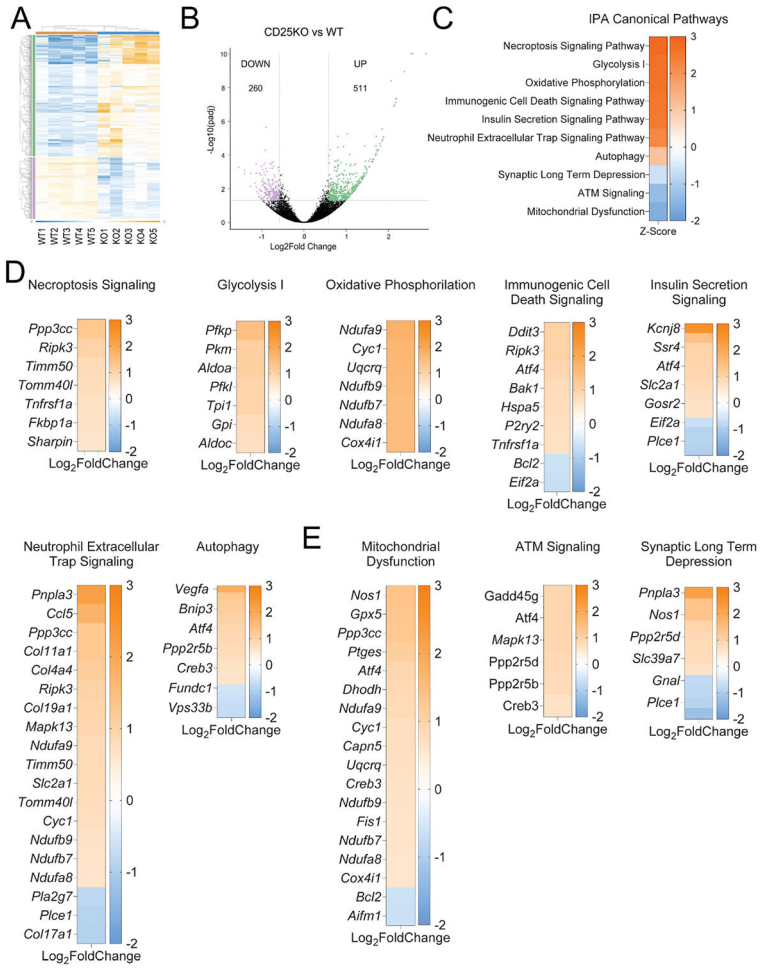

Fig. 3. Transcriptome changes in the corneal epithelium of CD25KO mice.

A. The overall heat map profile for 770 differentially expressed genes in the corneal epithelium. The samples on the left are from wild-type (n = 5, WT) and the ones from the right are from CD25KO mice (n = 5, KO).

B. A volcano plot showing the magnitude of change in the corneal epithelium modulated by CD25 expression (log 1.5-fold change) versus the adjusted p-value (−log10). The dotted line indicates a significance of 0.05.

C. Detailed heatmap of Z-scores of some canonical pathways identified using IPA.

D-E. Detailed heatmaps showing the mean of significantly differentially expressed genes (DEGs) associated with different upregulated pathways (D) and downregulated pathways (E). There were 5 samples/group that were averaged.

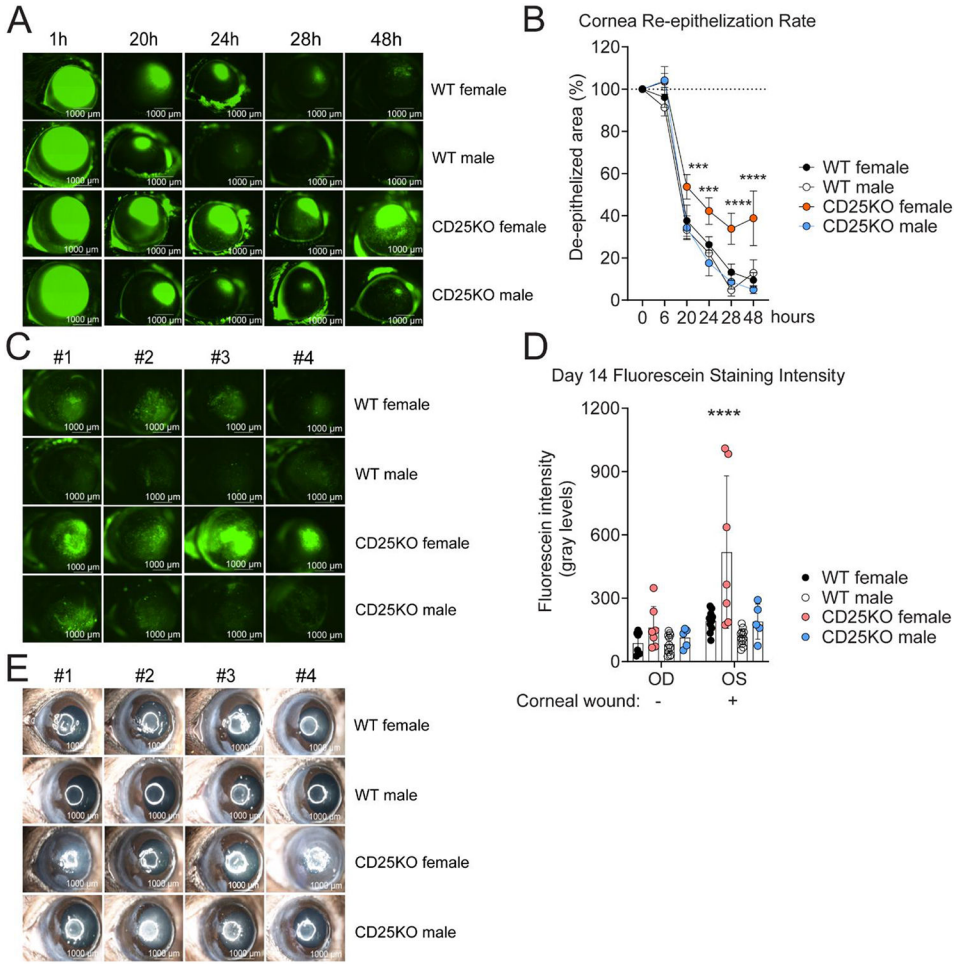

Fig. 4. Female CD25KO mice have delayed wound healing post-injury.

A 1.5mm unilateral injury was created in the left eye with a dull blade under general anesthesia. Mice were allowed to recover and were photographed at specific time points after the surgery. The size of the epithelial injury at 1h was set at 100%. A. Representative images of corneas stained with 0.1% sodium fluorescein post-corneal debridement in wild-type (WT) and CD25KO mice of both sexes at different time points post-injury as marked. F = female, M = male

B. Rate of re-epithelization in the experimental groups, n = 9-15/group (15 wild-type females; 12 wild-type males; 9 CD25KO females; 12 CD25KO males).

C. Representative images of corneas stained with 0.1% sodium fluorescein at 14 days post-corneal debridement in wild-type (WT) and CD25KO mice of both sexes.

D. Cumulative data of corneas stained with 0.1% sodium fluorescein 14 days post-injury. Kruskal-Wallis with Sidak's test, n = 6-10/group, each dot represents one eye, ****P < 0.0001

E. Bright field images of corneas shown in D before fluorescein staining.

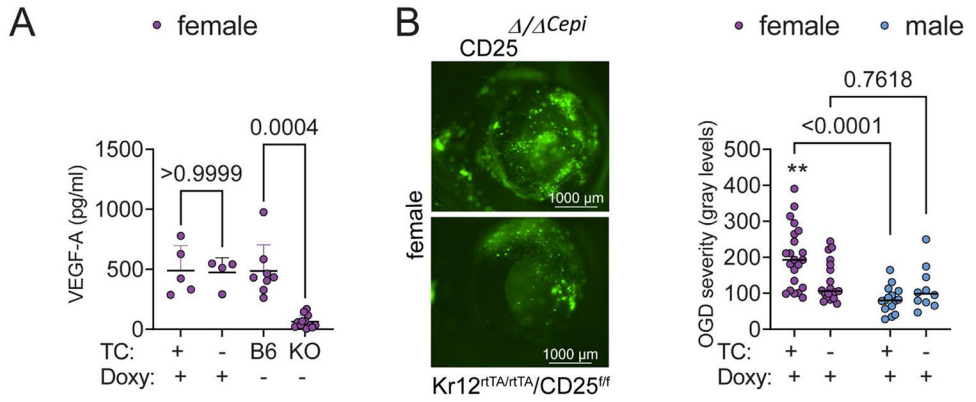

Fig. 5. Conditional deletion of CD25 in the cornea leads to spontaneous ocular surface disease.

A. Luminex assay showing protein levels of VEGF in tears. Each dot represents tear washing pooled from 4 eyes (2 mice); n = 5-13. Kruskal-Wallis with Dunn's multiple comparison test. P value as shown.

B. Representative images of female CD25$^{\Delta/\Delta Cepi}$ and Krt12$^{rtTA/rtTA}$/CD25$^{f/f}$ stained with Oregon-Green-Dextran (OGD) dye. Cumulative data is shown on the right. Two-way ANOVA with Sidak's posthoc test, P value as shown. Each dot represents one mouse (average of left and right eyes). Asterisk compares CD25$^{\Delta/\Delta Cepi}$ vs. Krt12$^{rtTA/rtTA}$/CD25$^{f/f}$. **P < 0.01. TC = TetOCre; Doxy = doxycycline diet; TC^{+}, Doxy^{+} = CD25$^{\Delta/\Delta Cepi}$; TC^{-}, Doxy^{+} = Krt12$^{rtTA/rtTA}$/CD25$^{f/f}$.

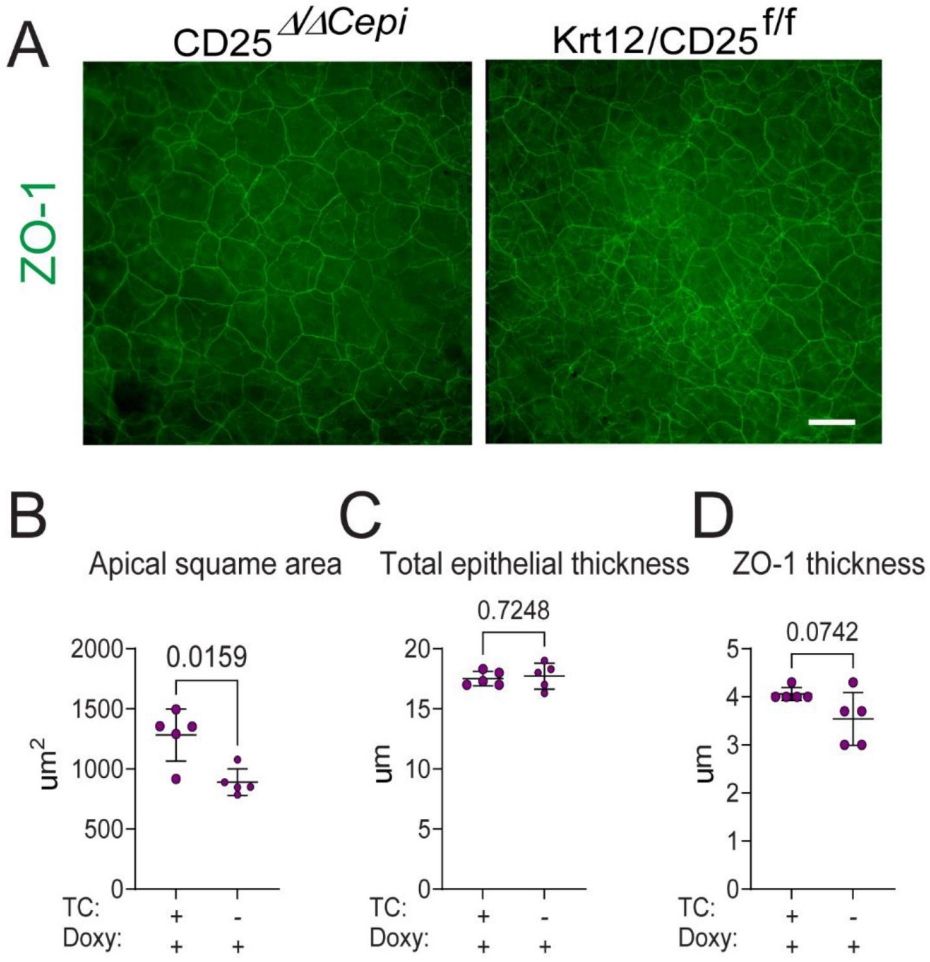

Fig. 6. Evaluation of tight junction proteins in the CD25$^{\Delta/\Delta Cepi}$ *mice*.

A. Representative laser scanning confocal microscopy showing wholemount corneas stained with ZO-1 (green) in female CD25$^{\Delta/\Delta Cepi}$ and Krt12$^{rtTA/rtTA}$/CD25$^{f/f}$ mice (n = 5/group). Bar graph = 25μm.

B. Cumulative squame area stained with ZO-1 and measured in NIS elements. At least 300 cells were averaged per eye per group (n = 5 individual corneas/group). Mann-Whitney U test.

C. Cumulative total epithelial thickness (n = 5 individual corneas/group). Mann-Whitney U test.

D. Cumulative ZO-1 thickness (n = 5 individual corneas/group). Mann-Whitney U test.

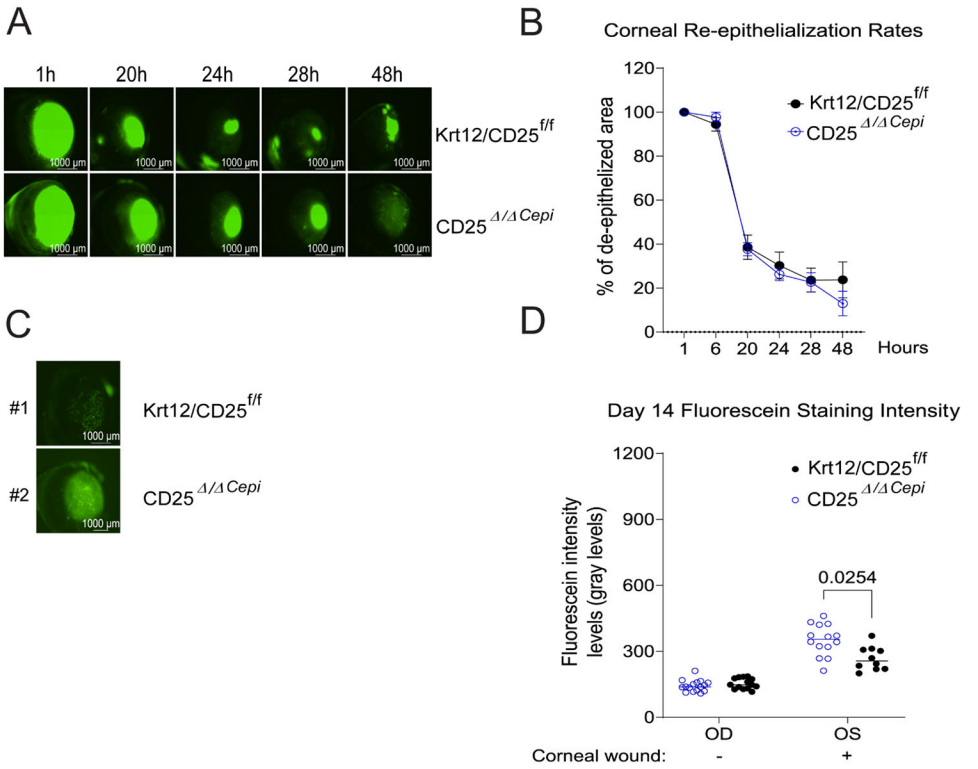

Fig. 7. Cornea-specific deletion of CD25 does not affect wound healing after corneal debridement but leads to residual barrier disruption post-wound.

A 1.5mm unilateral injury was created in the left eye with a dull blade under general anesthesia. Mice were allowed to recover and were photographed at specific time points after the epithelial debridement. The size of the epithelial injury at 1h was set at 100%.

A. Representative images of corneas stained with 0.1% sodium fluorescein post-corneal debridement in female $CD25^{\Delta/\Delta Cepi}$ *and* $Krt12^{rtTA/rtTA}/CD25^{f/f}$ mice at different time points post-injury as marked.

B. Rate of re-epithelization in the experimental groups (n = 18-20/group)

C. Representative images of corneas stained with 0.1% sodium fluorescein post-corneal debridement in female $CD25^{\Delta/\Delta Cepi}$ *and* $Krt12^{rtTA/rtTA}/CD25^{f/f}$ mice at 14 days post-injury

D. Cumulative data of corneas stained with 0.1% sodium fluorescein 14 days post-injury. Kruskal-Wallis with Sidak's multicomparison test. Each dot represents a left or right cornea, as marked, n = 10-20.

OD = right eye; OS = left eye

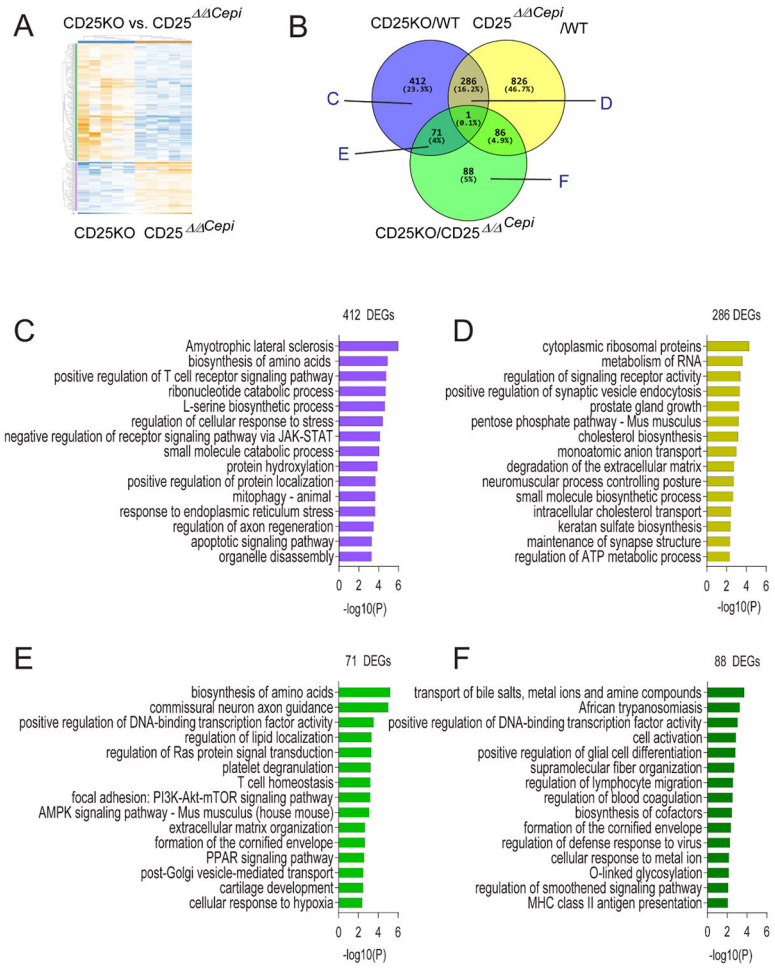

Figure 8. Comparison of CD25KO vs. CD25 $^{\Delta/\Delta CEpi}$ transcriptome changes in the corneal epithelium

A. The overall heat map profile for 246 differentially expressed genes in the corneal epithelium comparing CD25KO and CD25$^{\Delta/\Delta Cepi}$. The samples on the left are from CD25KO (n = 5) and the ones from the right are from CD25$^{\Delta/\Delta Cepi}$ mice (n = 5).

B. The number of differentially expressed genes (DEGs) in the different groups as depicted using a Venn diagram. Letters C,D,E, F indicate the pathways and are shown in the next graphs.

C-F Metascape analysis showing enriched pathways in the DEGs according to the Venn diagram in B.

Table 1:

List of used antibodies in this study.

Antibody Type	Target	Clone	Host	Reaction	Dilution (IF/WB)	Conjugation	Company (Catalog No.)
Primary	Krt12	Polyclonal	Rabbit	Mouse	1:100	No Conjugation	A kind gift from Winston-Kao
Primary	IL-2Rα (CD25)	7D4	Rat	Mouse	1:240	No Conjugation	BioLegend (154202)
Primary	IL-2Rβ (CD122)	Polyclonal	Rabbit	Mouse	1:100	No Conjugation	Proteintech (13602-1-AP)
Primary	IL-2Rγ (CD132)	Recombinant Monoclonal	Rabbit	Mouse	1:100	No Conjugation	ThermoFisher (MA5-29720)
Primary	Beta-actin	AC-15	Mouse	Mouse	1:5000	No conjugation	Sigma (AS441)
Secondary	IgG (H+L)	Polyclonal	Goat	Rat	1:1000	AlexaFluor® 594	Jackson ImmunoResearch (112-585-003)
Secondary	IgG (H+L)	Polyclonal	Goat	Rat	1:1000	AlexaFluor® 488	Jackson ImmunoResearch (112-545-003)
Secondary	IgG (H+L)	Polyclonal	Goat	Rabbit	1:1000	AlexaFluor® 594	Jackson ImmunoResearch (111-585-003)
Secondary	IgG (H+L)	Polyclonal	Goat	Rat	1:1000	HRP	Abcam (ab97057)
Secondary	IgG (H+L)	Polyclonal	Goat	Mouse	1:1000	HRP	Abcam (ab6789)